CUMULANTS ASSOCIATED WITH GEOMETRIC PHASES AND THEIR IMPLEMENTATION IN MODERN THEORY OF CRYSTALLINE POLARIZATION

A THESIS SUBMITTED TO

THE GRADUATE SCHOOL OF ENGINEERING AND SCIENCE

OF BILKENT UNIVERSITY

IN PARTIAL FULFILLMENT OF THE REQUIREMENTS FOR

THE DEGREE OF

MASTER OF SCIENCE

IN

PHYSICS

By

Sertac Cengiz

September 2022

Cumulants associated with geometric phases and their implementation
in modern theory of crystalline polarization
By Sertac Cengiz
September 2022

We certify that we have read this thesis and that in our opinion it is fully adequate, in scope and in quality, as a thesis for the degree of Master of Science.

Balazs Hetenyi(Advisor)

Ceyhun Bulutay

Menderes Işkın

Approved for the Graduate School of Engineering and Science:

Orhan Arıkan
Director of the Graduate School

ABSTRACT

CUMULANTS ASSOCIATED WITH GEOMETRIC PHASES AND THEIR IMPLEMENTATION IN MODERN THEORY OF CRYSTALLINE POLARIZATION

Sertac Cengiz
M.S. in Physics
Advisor: Balazs Hetenyi
September 2022

Many fields have been influenced by Berry's geometric phase because of its physical meaning and observable effects. One of the breakthroughs that stem from geometric phases is the modern theory of polarization. The expectation value of the position was not possible to calculate for crystalline structures because of ill-defined position operator. The modern theory of polarization showed that the geometric phase obtained by Zak phase, integral across the Brillouin zone, gives the first cumulants so that polarization is obtainable by the geometric phase. This indicates that cumulants are essential for studies such as polarization, charge transport, and electron localization. In the context of the modern theory of polarization, gauge-invariant cumulants are derived but they are not geometric even though they are physically well defined. In order to deal with this issue, a Binder cumulant associated with the adiabatic cycle is introduced, so called geometric Binder cumulant. Since the definition of Binder cumulants is based on a ratio of two cumulants, it is possible to eliminate factors that prevent the quantity to become geometric. An alternative way to extract cumulants associated with the adiabatic cycle is proposed as well. Error terms of the Cumulants are improved when they are extracted in an alternative way. Distortion around the transition points which modern theory of polarization has been reduced significantly. Geometric Binder cumulant is implemented to observe the difference between gapped and gapless band structures. One-dimensional and two-dimensional models are investigated and phase transition between metallic and insulating states is clearly observed. SSH model is investigated to make a comparison with the modern theory of polarization and development in the

formalism is shown. Geometric Binder cumulant also lets us observe the correlated model and a method based on renormalization group theory is used to locate transition points in the correlated model. Results are in good agreement with each other. An alternative way to extract cumulants is also extended to two-dimensional systems and phase transition is observed in two-dimensional systems with the usage of geometric Binder cumulant. Regardless of whether the two-dimensional system has a zero-dimensional or one-dimensional Fermi surface, Geometric Binder cumulant is a quantity that is sensitive for the metallic and insulating cases. For the open gap case, geometric Binder cumulant is affected by the system size, and the effect of the system size is distinct. An increase in the system size improves the quantity.

Keywords: Adiabatic cycle, Binder cumulant, Cumulants, Crystalline polarization, Phase transition.

ÖZET

GEOMETRİK FAZLAR İLE İLİŞKİLİ KÜMÜLANTLAR VE MODERN KRİSTAL POLARIZASYON TEORİSİNDEKİ UYGULAMALARI

Sertac Cengiz
Fizik, Yüksek Lisans
Tez Danışmanı: Balazs Hetenyi
Eylül 2022

Fiziksel anlamı ve gözlemlenebilir etkileri nedeniyle birçok alan Berry'nin geometrik fazından etkilenmiştir. Geometrik fazdan kaynaklanan atılımlardan biri modern polarizasyon teorisidir. Konumun beklenen değeri, kötü tanımlanmış sınırlar nedeniyle kristal yapılar için hesaplamak mümkün değildi. Modern polarizasyon teorisi, adyabatik döngü ile elde edilen geometrik fazın ilk kümülantları verdiğini, böylece polarizasyonun geometrik faz ile elde edilebileceğini göstermiştir. Bu durum, kümülantların polarizasyon, yük taşıma, elektron lokalizasyonu gibi çalışmalar için gerekli olduğunu göstermektedir. Modern polarizasyon teorisi bağlamında, ölçü değişmez kümülantları türetilmiştir, ancak fiziksel olarak iyi tanımlanmış olmalarına rağmen geometrik değildirler. Bu sorunu çözmek için, geometrik Binder kümülantı olarak adlandırılan adyabatik döngü ile ilişkili Binder kümülantlar tanıtıldı. Binder kümülantı tanımı iki kümülantın oranına göre yapıldığından tanımın geometrik hale gelmesini engelleyen faktörleri ortadan kaldırmak mümkündür. Adyabatik döngü ile ilişkili kümülantları elde etmenin alternatif bir yolu da önerilmiştir. Cumulantların hata terimleri, alternatif yolla elde edildiğince iyileşir. Modern polarizasyon teorisinin sahip olduğu geçiş noktaları etrafındaki bozukluklar önemli ölçüde azalır. Aralıklı ve arılıksız bant yapıları arasındaki farkı gözlemlemek için Geometric Binder kümülant uygulanmıştır. Bir boyutlu ve iki boyutlu modeller incelenmiş ve metalik ve yalıtkan hal arasındaki faz geçişi açıkça gözlemlenmiştir. SSH modelinde modern polarizasyon teorisi ile karşılaştırma yapmak için araştırılmış ve formalizmdeki gelişme gösterilmiştir. Geometrik Bağlayıcı kümülatı ayrıca ilişkili modelleri gözlemlememizi sağlar ve ilişkili modeldeki geçiş noktalarını bulmak için renormalizasyon grubu teorisine dayalı bir yöntem de kullanılmıştır. Sonuçlar birbirleriyle iyi bir uyum içindedir. Kümülantları çıkarmanın alternatif yolu iki

boyutlu sistemlere de genişletilmiştir ve geometrik Binder kümülatı kullanılarak faz geçişi iki boyutlu sistamlerde de gözlenmiştir. iki boyutlu sistemin sıfır boyutlu veya tek boyutlu Fermi yüzeyi olduğuna bakılmaksızın geometrik Binder kümülantı metalik ve yalıtkan duruma duyarlı bir niceliktir. Arılıklı bant durumunda, geometrik Binder kümülantı sistem boyutundan etkilenir ve sistem boyutundan kaynaklanan etki belirgindir. Sistem boyutundaki artış niceliği geliştirir.

Anahtar sözcükler: Adyabatik döngü, Binder kümülant, Kümülantlar, Kristal polarizasyon, Faz geçişi.

Acknowledgement

First of all, I would like to express my deepest and most sincere thanks to my advisor Prof. Balazs Hetenyi. He was always kind and helpful. Thanks to our discussions with him and his guidance, I was able to carry out my work. I would like to thank all the professors who supported and taught me, especially Prof. Özgür Oktel, Prof. Ceyhun Bulutay and Prof. Ahmet Züfer Eriş. Thanks to them, my knowledge has increased and my perspective has widened. I would also like to thank my close friends such as Ayşenur Atikeler, Yetkin Pulcu and Selçuk Parlak. They were always there for me and supported me.

Dedicated to Karaca.

Contents

List of Figures

List of Tables

Chapter 1

Introduction

Berry's geometric phase [1] which was published in 1984 was very influential in many fields. The geometric phase is a physical phenomenon and observable effect in numerous cases since it is gauge-invariant. For the crystalline systems in thermodynamic limits, Zak defined the geometric phase over a loop across the Brillouin zone [2]. Topological invariants are constructed based on this geometric phase and it characterizes topological insulators' phases [3–7]. Another development led by Zak phase was made in electric polarization by associating it with adiabatic charge transport [8–10]. The geometric phase is also correlated with gauge field theories and differential geometry so this important property provides an explanation for the quantum Hall effect whose formulation corresponds with integer Chern numbers [11–13]. The first example of a topological insulator is Haldane's study on the integer quantum Hall effect which is a Chern insulator on hexagonal lattice [7, 14]. In the study of charge transport, cumulants are crucial because they are related to quantities such as the variance of the polarization [10], shift current [15] through sum rules. Cumulants are necessary for the modern theory of polarization [16, 17] and the geometric phase is considered as the first members of cumulants that are extracted from the adiabatic cycle.

Souza, Wilkens, and Martin derived gauge-invariant cumulants in the context of the modern theory of polarization [18]. Although cumulants defined by Souza,

Wilkens, and Martin are physically well defined, they are not geometric. In this work, a quantity is demonstrated that is physically well defined as well as geometric. This is achieved by taking a ratio of two gauge invariant cumulants associated with an adiabatic cycle in a particular way. This way is very similar to the Binder cumulants [19, 20]. Binder cumulant is obtained with the ratio of the fourth cumulant (kurtosis) by the square of the second cumulant (variance). Because of its construction, Binder cumulant is applied to the finite size scaling hypothesis [21]. At transition points, the size dependency of cumulants is canceled in the ratio, and Binder cumulant becomes independent of size. In the numerical calculations, phase transition points are affected by the finite size, and obtaining some critical points or calculating some parameters don't become accurate well. Using Binder cumulant eliminates the effects stemming from the finite size at transition points. Binder cumulant is useful in both classical [22] and quantum [23] transition points. Binder cumulant is constructed associated with adiabatic cycle and called geometric Binder cumulant (GBC). This method is implemented in the modern theory of polarization.

In this thesis, extraction of cumulants from polarization amplitude Z_q is studied as well. It is argued that Z_q is the characteristic function for crystalline systems. In the standard way, a discrete logarithmic derivative is taken to extract cumulants. Instead of the standard way, the original Resta-Sorella method [10,24] is modified and an alternative way is proposed to extract cumulants. With this alternative way, cumulants are extracted with finite difference derivatives of Z_q whose phase is removed. Construction in this work is based on this method. This discussion is also extended to two-dimensional polarization amplitude and a scheme is developed to distinguish transition points for two-dimensional systems.

There are many different scaling laws and several of them have been used for ages. Besides the size scaling approach, another scaling argument is the renormalization group and it was developed to scale transformations in quantum electrodynamics [25, 26]. Recently, this method is applied to real-space renormalization to the polarization amplitude [27]. Consider a correlated model, the system can be renormalized and a new system can be formed. This scales the Hamiltonian to a new one. After enough iteration, the critical point is found. This idea is

implemented to renormalize a correlated model and scale polarization amplitude Z to determine the phase transition point.

In Chapter 2, the Geometric (Berry's) phase is presented. Then modern polarization is explained and extraction of cumulants is given. Geometric Binder cumulant is also defined in this chapter. Investigated models are examined in Chapter 3. One-dimensional (SHH model with two different impurities) and two-dimensional models (Graphene and Haldane models) are investigated. In Chapter 4, calculation methods are discussed. The Alternative way to extract cumulants and approach for two-dimensional polarization amplitude is defined in this chapter. Results are shown and analyzed in Chapter 5. The thesis is concluded with Chapter 6.

Chapter 2

Polarization and Cumulants

Geometric phase is very influential for many fields. Concept of modern theory of polarization [16, 17] is crucially based on geometric phase. The idea relies on the quantum adiabatic transport of particles. Geometric phase is derived for a particle which acts on a Hamiltonian evolution under adiabatically changing parameters. Geometric phase is considered the first member of cumulants. Therefore, modern theory of polarization stems from cumulants which are extracted from adiabatic cycle [9,10]. Gauge invariant cumulants are derived in the context of modern theory of polarization [18] but they are not geometric although they are physically well defined. This problem is overcome with geometric Binder cumulant (GBC), which is a Binder cumulant based on adiabatic cycle.

2.1 Geometric Phase

Phase factor is obtained as a result of adiabatic approximation. During diabatic process, conditions are changing rapidly so system cannot adapt. Therefore, eigenstates which system start with will not end in the eigenstates of the final Hamiltonian. In adiabatic approximation, parameters which Hamiltonian of the system depends on are slowly changing. This slow change allows system to adapt

to conditions. During adiabatic process, eigenstates of the initial Hamiltonian follow the eigenstates of Hamiltonian which we get from the Hamiltonian with changed parameters. For example, if we start spin pointing in r_0 direction parallel to B field and gradually rotate B to direction r, according to adiabatic theorem the spin will also point in r direction.

In order to derive adiabatic theorem, expand a state $|\Psi(t)\rangle$ in terms of the instantaneous eigenstates $\{|n(t)\rangle\}$ of $\hat{H}(t)$.

$$H(t)|n(t)\rangle = E_n(t)|n(t)\rangle. \tag{2.1}$$

$$|\Psi(t)\rangle = \sum_n c_n(t)|n(t)\rangle. \tag{2.2}$$

Schrödinger's wave equation with this state yields,

$$i\hbar\frac{\partial}{\partial t}|\Psi(t)\rangle = H(t)|\Psi(t)\rangle. \tag{2.3}$$

Substituting with the expansion (2.2), wave equation (2.3) becomes,

$$i\hbar\sum_n(\dot{c}_n(t)|n(t)\rangle + c_n(t)|\dot{n}(t)\rangle) = \sum_n c_n(t)E_n(t)|n(t)\rangle. \tag{2.4}$$

Projecting it with $\langle k(t)|$ gives,

$$i\hbar\dot{c}_k(t) + i\hbar\sum_n c_n(t)\langle k(t)|\dot{n}(t)\rangle = c_k(t)E_k(t). \tag{2.5}$$

We need to evaluate second term in the left sight of the equation (2.5). In order to evaluate it, we will take time derivative of equation (2.1).

$$\dot{H}(t)|n(t)\rangle + H(t)|\dot{n}(t)\rangle = \dot{E}_n(t)|n(t)\rangle + E_n(t)|\dot{n}(t)\rangle. \tag{2.6}$$

When we project it with $\langle k(t)|$, then we get,

$$\langle k(t)|\dot{H}(t)|n(t)\rangle + E_k(t)\langle k(t)|\dot{n}(t)\rangle = \dot{E}_n(t)\delta_{k,n} + E_n(t)\langle k(t)|\dot{n}(t)\rangle. \tag{2.7}$$

For $n = k$, we have $\langle k|\dot{H}|k\rangle = \dot{E}_k$. It is also known as the Hellmann-Feynman theorem. When $n \neq k$, we have $\langle k|\dot{n}\rangle = \frac{\langle k|\dot{H}|n\rangle}{E_n - E_k}$. After substituting equivalent of $\langle k|\dot{n}\rangle$ into equation (2.5), it yields,

$$i\hbar\dot{c}_k(t) = c_k(t)(-i\hbar\langle k(t)|\dot{k}(t)\rangle + E_k(t)) - i\hbar\sum_{n\neq k} c_n(t)\frac{\langle k(t)|\dot{H}(t)|n(t)\rangle}{E_n(t) - E_k(t)}. \tag{2.8}$$

First term is called adiabatic term and second term is called error term. Error term can be neglected under adiabatic approximation. According to adiabatic theorem, if $\left|\hbar\langle k(t)|\dot{H}(t)|(t)\rangle\right| \ll \min_t[E_n(t) - E_k(t)]^2$, transitions between level n and k are suppressed. Solution of $i\hbar\dot{c}_k = c_k(-i\hbar\langle k|\dot{k}\rangle + E_k)$ gives,

$$\begin{aligned} c_k(t) &= c_k(t=0)e^{i\theta_k(t)}e^{i\gamma_k(t)}, \\ |\Psi(t)\rangle &= e^{i\theta_k(t)}e^{i\gamma_k(t)}|n(t=0)\rangle. \end{aligned} \tag{2.9}$$

where ,

$$\theta_k(t) = -\frac{1}{\hbar}\int_0^t E_k(t')dt', \qquad \gamma_k(t) = i\int_0^t \langle k(t')|\frac{d}{dt'}k(t')\rangle dt'. \tag{2.10}$$

θ is the Dynamical phase and γ is the geometric phase, which is also known as Berry phase if the process is cyclic. Dynamical phase is ordinary phase expected for energy eigenstates. However, geometric phase is the surprising part and it is a topological phase factor. Let's represent time dependence of the Hamiltonian by a vector $R(t)$. By chain rule, time derivative of $|k(t)\rangle$ gives; $\frac{d}{dt}|k(R(t))\rangle = \sum_i \frac{d}{dR_i}|k(R(t))\rangle \frac{dR_i}{dt} = \nabla_R |k(R(t))\rangle \frac{dR}{dt}$. Then, Berry phase γ becomes,

$$\gamma_k(R(t)) = i\int_0^t \langle k(R(t'))|\nabla_R|k(R(t'))\rangle \frac{dR}{dt'}dt' = i\int_{R(t=0)}^{R(t)} \langle k(R(t'))|\nabla_R|k(R(t'))\rangle dR. \tag{2.11}$$

In the case where t represents the period for one full cycle, so that $R(0) = R(t)$ and equation (2.11) gives the phase difference along the closed path. Otherwise, phase is along the open path. In this closed path case, Berry phase is gauge invariant and observable.

$$\gamma_k = i\oint_C \langle k(R)|\nabla_R|k(R)\rangle dR. \tag{2.12}$$

Phase difference can be also defined with discrete loop. In the limiting case, total phase difference over closed path converges to closed integral, i.e. $\sum \Delta\varphi \longrightarrow \oint_C d\varphi$ where $\oint_C d\varphi = \gamma$. Phase difference between two state will be defined as $\Delta\varphi_{s,s+1} = \langle \phi(\xi)|\phi(\xi + \Delta\xi)\rangle$ with arbitrary discrete parameter ξ. Sum of the each phase between two states along the continuous path will give the phase difference of the path.

$$\gamma = \sum_{s=1}^{N} \Delta\varphi_{s,s+1}. \tag{2.13}$$

The term $A_k(R)dR = i\langle k(R)|\nabla_R|k(R)\rangle$ is defined as Berry connection and then Berry phase can be written as $\gamma_k = \oint A_k(R)dR$. Using the Stokes' theorem,

it can be also expressed as; $\gamma_k = \oint A_k(R)dR = \int(\nabla_R \times A_k(R))da$ where $B_k(R) = \nabla_R \times A_k(R)$ is called Berry curvature. Thus, Berry phase is determined by the flux of a generalized field. Closed path Berry phase is significant observable in many areas. Modern polarization theory is based on it so that it plays important role for modern electronic structure theory.

2.2 Modern Theory of Polarization

Dipole moment of a finite one dimensional electron system which has wave function Ψ and the electron density function $n(x)$ can be written as,

$$p = q\langle x\rangle = q\int dx\; xn(x) = q\langle\Psi|\hat{X}|\Psi\rangle. \tag{2.14}$$

Dipole moment is the central quantity for very essential concepts such as polarization. Knowledge of the electronic distribution should be enough for macroscopic polarization in the thermodynamic limit and macroscopic polarization should be insensitive to surface effects. With the classical way, dipole moment is described within a unit cell. Consider a macroscopic solid. If we assume that system is discrete and well separated, then using equation (2.14) will fail because of the incorrect definitions. Suppose that we have long one dimensional lattice which has two sub-lattices where one sub-lattice consist of anions and the other sub-lattice consists of cations. Two different unit cells can be chosen, anion-cation or cation-anion. Dipole moments of these two unit cell are different and dipole moment of the system will not be obtained. Attempt fails because position operator is ill defined. Calculation of the dipole moment by using equation (2.14) for periodic crystal is affected by surface. The solution to the problem is built starting by dealing with the position operator. Consider an electron in one-dimensional system which has periodic boundary condition, i.e. $\Psi(x+L) = \Psi(x)$ where L is imposed periodicity. Assume that distribution has a center x_0 in the domain $(0, L)$ then it periodically repeats. In order to deal with the position

operator, complex number z which consists of quantity $\exp(i2\pi x/L)$ is defined as,

$$z = \langle\Psi(x)|e^{i(2\pi/L)\hat{x}}|\Psi(x)\rangle = \int_0^L dx\ e^{i(2\pi/L)\hat{x}}|\Psi(x)|^2. \tag{2.15}$$

In the extreme delocalization case, we have electron density $|\Psi|^2 = 1/L$ so that amplitude z is 0. In the extreme localization at centers case, we have following electron density,

$$|\Psi(x)|^2 = \sum_{m=-\infty}^{\infty} \delta(x - x_0 - mL). \tag{2.16}$$

and then z becomes $\exp(i2\pi x_0/L)$. Therefore, electron density can be written in term of a density function n_{loc} for general location case where function n_{loc} satisfies the above extreme cases.

$$|\Psi(x)|^2 = \sum_{m=-\infty}^{\infty} n_{loc}(x - x_0 - mL). \tag{2.17}$$

Equation (2.17) can be substituted into equation (2.15). This expression can be considered as a Fourier transform of the n_{loc} and then z can be considered in terms of this Fourier transform $\tilde{n}_{loc}$.

$$z = e^{i(2\pi/L)x_0}\tilde{n}_{loc}\left(-\frac{2\pi}{L}\right). \tag{2.18}$$

Difference between delocalised and localised cases becomes apparent under examination of z's behavior. For delocalised case, z depends on L while z is independent from L for localised case. If localization is close to extreme localization, Fourier transform $\tilde{n}_{loc}$ can be expanded as follows,

$$\tilde{n}_{loc}\left(-\frac{2\pi}{L}\right) = 1 - \frac{1}{2}\left(\frac{2\pi}{L}\right)^2 \int_{-\infty}^{\infty} dx\; x^2 n_{loc}(x) + O(L^{-3}). \tag{2.19}$$

It is clear that $|z|$ goes to 1 while L is increasing. As a result of that, expectation value can be obtained by the phase of the z.

$$\langle x \rangle = \frac{L}{2\pi} \operatorname{Im} \ln z. \tag{2.20}$$

Since system is periodic over L, expectation value is proportional to L. Now, we have expectation value and polarization (2.14) can be calculated. Comparing it with the equation (2.12), it is clearly seen that expectation value is multiple of Berry phase. For a many-particle system, assume that there are N electrons and system size is L. Thermodynamic limit is considered. N and L go to infinity and ratio between them N/L is equal to finite density of electron n. In this case, state obeys conditions for each particle variable separately. Many-body operator will be defined as $X = \sum_i^N x_i$. Then z will be defined as,

$$z_N = \langle \Psi(x) | e^{i(2\pi/L)\hat{X}} | \Psi(x) \rangle. \tag{2.21}$$

Expectation value becomes as follow,

$$\langle X \rangle = \frac{L}{2\pi} \operatorname{Im} \ln z_N. \tag{2.22}$$

On the other hand, equation (2.18) can be used to calculate the variance of the electron distribution. Taylor series centered at 1 gives $(z-1)$ for the first term of the summation expansion. It can be assumed that $\ln |z|$ is approximately equal to second term of equation (2.19).

$$\ln|z| \simeq -\frac{1}{2}\left(\frac{2\pi}{L}\right)^2 \int_{-\infty}^{\infty} dx\, x^2 n_{loc}(x). \tag{2.23}$$

Then, variance of the electron distribution can be defined as,

$$\sigma^2 = \langle x^2\rangle - \langle x\rangle^2 = -\left(\frac{L}{2\pi}\right)^2 \ln|z|^2. \tag{2.24}$$

Equation (2.24) provides alternative way to examine localised cases. As it was discussed above, While system is getting localised, n_{loc} becomes more L independent. $|z|$ goes to constant limit and it becomes proportional to L^2. As a result, it is expected that the size-scaling exponent is two for the delocalised system.

2.3 Cumulants

Assume that $w(x)$ is the probability density of random variable X where $w(x)dx$ gives the probability of variable X which takes on the value x in the interval $[x, x+dx]$. The mean value of X is defined as,

$$\langle X\rangle = \int_{-\infty}^{\infty} dx w(x) x. \tag{2.25}$$

This is the first moment of the probability density and the mean value of X's powers provides other moments. The nth moment is defined as, $M_n = \langle X^n\rangle$. Characteristic function is defined as Fourier transform of the probability density.

$$z(k) = \int_{-\infty}^{\infty} dx e^{-ikx} w(x). \tag{2.26}$$

Consider the power series expansion of e^{at}. nth derivative of e^{at} with respect to the a where a goes to zero gives nth power of t.

$$\frac{\partial^n e^{at}}{\partial t^n} \mid_{a=0} = t^n. \tag{2.27}$$

Therefore, nth moment will be found by multiplying nth derivative of characteristic function (2.26) by $(i)^n$. Characteristic function which is defined in terms of the moments can be redefined by taking the logarithm of the expansion in moments. The expansion coefficients are called cumulants. Therefore, cumulants can found by nth derivative of logarithm of the characteristic function. Characteristic function Z_q is a discrete analog of a characteristic function, at integral values of q and is defined as,

$$Z_q = \langle \Psi(x) | e^{i(2\pi q/L)\hat{X}} | \Psi(x) \rangle. \tag{2.28}$$

This characteristic function can be calculated with cyclic product in discrete form.

$$Z_q = \prod_{q=1}^{N} \langle \Psi(x) | \Psi(x+q) \rangle. \tag{2.29}$$

Generating moments and cumulants with characteristic function Z_q will follow as,

$$M_n = \left(\frac{L}{2\pi i} \right)^n [Z_q]_{q=0}^{(n)}, \tag{2.30}$$

$$C_n = \left(\frac{L}{2\pi i} \right)^n [\ln Z_q]_{q=0}^{(n)}. \tag{2.31}$$

Due to periodicity, the domain of q is discrete so that one can only take the discrete derivatives and the notation $[f_q]^{(n)}_{q=0}$ means discrete derivative of order n of the function f_q at $q = 0$.

2.3.1 Binder Cumulant

Consider the phase calculation based on discrete cyclic product with parameter space ξ.

$$Z_q = \prod_{m=1}^{N} \langle \phi(\xi_m) | \phi(\xi_{m+q}) \rangle. \tag{2.32}$$

To obtain cumulants, lets expand the $\ln Z$ with above discrete definition (2.32). First term of the expansion $_1$ will give the first moment, which is also equal to first cumulant.

$$C_1 = \mathrm{Im} \sum_{m=1}^{N} \Delta\xi \langle \phi(\xi_m) | \nabla_\xi | \phi(\xi_m) \rangle. \tag{2.33}$$

in continuous limit, it can be written as,

$$C_1 = \mathrm{Im} \oint d\xi \langle \phi(\xi_m) | \nabla_\xi | \phi(\xi_m) \rangle. \tag{2.34}$$

which is geometric phase which is also called Berry phase. Second term of the expansion lnZ_1 will give the second moment and second cumulant will be obtained as following,

$$C_2 = -\sum_{m=1}^{N} \Delta\xi^2 \left[\langle \phi(\xi_m) | (\nabla_\xi)^2 | \phi(\xi_m) \rangle - (\langle \phi(\xi_m) | \nabla_\xi | \phi(\xi_m) \rangle)^2 \right]. \tag{2.35}$$

In this case, in order to take continuous limit, one factor of the $\Delta\xi$ in the equation (2.35) has to be eliminated so that second cumulant can be written as follow,

$$\Gamma_2 = -\int d\xi \left[\langle\phi(\xi_m)|(\nabla_\xi)^2|\phi(\xi_m)\rangle - (\langle\phi(\xi_m)|\nabla_\xi|\phi(\xi_m)\rangle)^2\right]. \tag{2.36}$$

Definition (2.36) is physically well defined but it is no longer geometric since one factor of the $\Delta\xi$ was eliminated. Same issue is valid for higher order cumulants. Binder cumulant is defined as,

$$U = 1 - \frac{C_4}{3C_2^2}. \tag{2.37}$$

Ratio of fourth cumulant and square of the second cumulant is a physically well defined construction and it gives gauge invariant quantity as well as being geometric. Fourth cumulant will be in term of four factor of $\Delta\xi$. All $\Delta\xi$ factors except one can be canceled in the ratio. Then continuous limit of cumulants will be left. This let us to construct Binder cumulant without eliminating any factor. Therefore, Binder cumulant based on adiabatic cycle gives possibility to obtain geometric quantity.

Chapter 3

Models

For one dimension, this formalism is implemented to Su-Schrieffer–Heeger (SSH) model [28]. It is the simplest model to investigate topological behaviour. System is localised by creating impurities with on-site potential or nearest neighbour interaction. Besides SSH model, it is also studied with two dimensional models. Lots of interest have been shown to graphene after it's discovery because of it's fundamental properties. Therefore, in the field topological insulators, graphene is also studied. Quantum Hall effect is shown in graphene [5] and first example of Chern insulator is given on a hexagonal lattice [7, 14].

3.1 SSH model with on-site potential

The Su-Schrieffer–Heeger (SSH) model is the simplest model to exhibit basic concepts of topological insulators. Model is based on one dimensional lattice which consisting of spinless fermions. In the system, particle hopping is regarded. System becomes trivial or topological in the way hopping strength is taken.

One dimensional lattice contain N unit cells and each unit cell contains two sublattices, where one contains particle A and other contains particle B. No particle interaction is considered. Adding on-site potential to the system is called

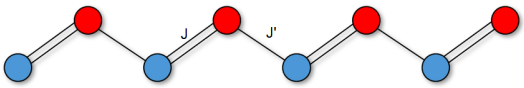

Figure 3.1: SSH model representation. Sub-lattice A and sub-lattice B are shown with different colour. J is the inter-cell hopping parameter and J' is intra-cell hoping parameter.

the Rice-Mele model. System Hamiltonian is defined as follow,

$$\hat{H} = J\sum_{m}(c^{\dagger}_{B,m}c_{A,m} + h.c.) + J'\sum_{m}(c^{\dagger}_{A,m+1}c_{B,m} + h.c.) \\ +\Delta\sum_{m}(c^{\dagger}_{A,m}c_{A,m} - c^{\dagger}_{B,m}c_{B,m}). \tag{3.1}$$

where J and J' are real hopping strengths of inter-cell and intra-cells, Δ is on-site potential. Operator $c^{\dagger}_{A,m}$ ($c_{A,m}$) creates (annihilates) particle in site m in sub-lattice A and operator $c^{\dagger}_{B,m}$ ($c_{B,m}$) creates (annihilates) particle in site m in sub-lattice B. In the thermodynamic limit, i.e. $N \to \infty$, $V \to \infty$, $N/V = constant$, fluctuations are negligible since the ratio of the size of the fluctuations to global quantities. However, even in the thermodynamic limit there are edge states. They appear as zero energy mode. Periodic boundary condition is implemented so that there is no edge states. Due to translational symmetry of the system, Bloch theorem can be applied. Bloch theorem states that eigenstates are defined in the form of plane wave regulated by periodic function in a system with periodic boundary conditions, $|\Psi(k)\rangle = |k\rangle \otimes |u(k)\rangle$. Fourier transformation is used to decompose into wave form. Fourier transforms of the operators follow,

$$c_k = \frac{1}{\sqrt{L}}\sum_{m} e^{imk}c_m, \qquad c_m = \frac{1}{\sqrt{L}}\sum_{k} e^{-imk}c_k. \tag{3.2}$$

Linear combination of operators in wave form is substituted into Hamiltonian. And following identity is considered, $c^{\dagger}_i c_j = \delta_{c_i,c_j}$.

$$\hat{H} = J\sum_m\sum_k(\frac{e^{imk}}{\sqrt{L}}c^\dagger_{B,k}\frac{e^{-imk}}{\sqrt{L}}c_{A,k} + h.c.) \tag{3.3}$$
$$+J'\sum_m\sum_k(\frac{e^{i(m+1)k}}{\sqrt{L}}c^\dagger_{A,k}\frac{e^{-imk}}{\sqrt{L}}c_{B,k} + h.c.)$$
$$+\Delta\sum_m\sum_k(\frac{e^{imk}}{\sqrt{L}}c^\dagger_{A,k}\frac{e^{-imk}}{\sqrt{L}}c_{A,k} - \frac{e^{imk}}{\sqrt{L}}c^\dagger_{B,k}\frac{e^{-imk}}{\sqrt{L}}c_{B,k}).$$

It yields Hamiltonian in the k-space form.

$$\hat{H} = J\sum_k(c^\dagger_{B,k}c_{A,k} + h.c.) + J'\sum_k(e^{ik}c^\dagger_{A,k}c_{B,k} + h.c.) \tag{3.4}$$
$$+\Delta\sum_k(c^\dagger_{A,k}c_{A,k} - c^\dagger_{B,k}c_{B,k}).$$

Hamiltonian can be written in matrix form as $\hat{H} = \sum_k c^\dagger_k\hat{h}(k)c_k$ where,

$$\hat{h}(k) = \begin{bmatrix} \Delta & J + J'e^{ik} \\ J + J'e^{-ik} & -\Delta \end{bmatrix}. \tag{3.5}$$

This approach simplifies the calculation of the system. Matrix form of the Hamiltonian (3.5) has two degrees of freedom. Any such two-level Hamiltonian can be written in terms of the Pauli matrices σ.

$$\hat{h}(k) = d_0(k)\hat{\sigma}_0 + d_x(k)\hat{\sigma}_x + d_y(k)\hat{\sigma}_y + d_z(k)\hat{\sigma}_z. \tag{3.6}$$

where $d(k)$ vectors are strength of the Pauli matrices. For the Hamiltonian (3.5), these strength vectors are,

$$d_0 = 0, \quad d_x = J + J'\cos(k), \quad d_y = J'\sin(k), \quad d_z = \Delta. \tag{3.7}$$

Ground state energy and its state for corresponding Hamiltonian (3.6) is

$$E_g = d_0 + d, \qquad |\Psi(k)\rangle = \begin{bmatrix} \sin(\theta(k)/2) \\ e^{-i\phi(k)} \cos(\theta(k)/2) \end{bmatrix}. \tag{3.8}$$

where $d = \sqrt{d_x^2 + d_y^2 + d_z^2}$ and angles defined as,

$$\theta(k) = \arccos(d_z/d), \qquad \phi(k) = \arctan(d_y/d_x). \tag{3.9}$$

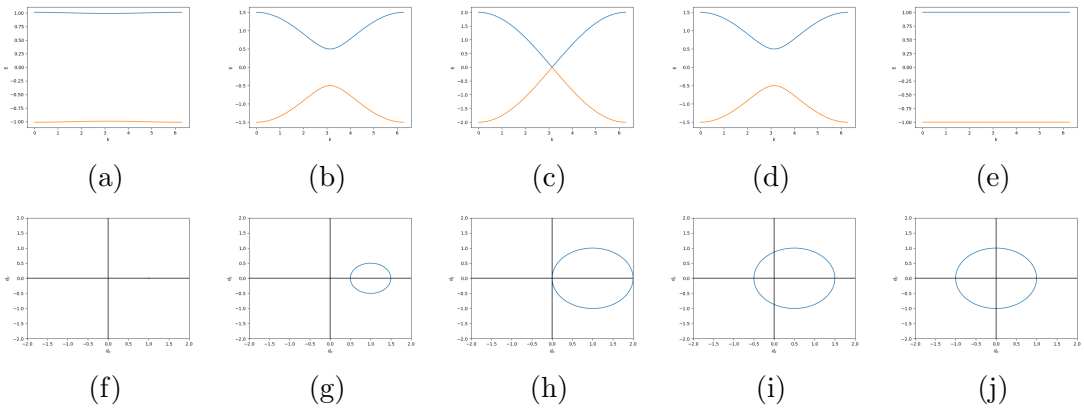

Figure 3.2: Hopping strengths are; (a),(f) $J = 1$ and $J' = 0$. (b),(g) $J = 1$ and $J' = 0.5$. (c),(h) $J = 1$ and $J' = 1$. (d),(i) $J = 0.5$ and $J' = 1$. (e),(j) $J = 0$ and $J' = 1$. Band gap is shown in (a),(b),(c),(d) and (e). Winding number is seen in (f),(g),(h),(i) and (j)

Assume that Δ is zero, so only J and J' affect the system. In the case where $J = J'$, gap between energy bands is closed so system is conductor. Otherwise, i.e. $J \neq J'$, gap is open and system becomes insulator. d_x and d_y vectors give idea for topology of the system by evaluating winding number, which is total number of closed curve travels counterclockwise around a point. When $J > J'$, winding number around origin is zero so system is topologically trivial. On the other hand, when $J < J'$, winding number is one so system is topological. With the condition $J = J'$, topological transition occurs and this is the case in which system is not insulator.

3.2 t-V correlated model

Particle interaction is a significant phenomenon. In order to basically examine affect of particle interaction, simple toy model is used. Nearest neighbour (n.n.) interaction is added to SSH model. Inter-cell and intra-cell hopping strengths are taken equal to each other. Hamiltonian of such system follows,

$$\hat{H} = -t \sum_{m} (c_{m+1}^{\dagger} c_m + h.c.) + V \sum_{m} n_m^{\dagger} n_{m+1}. \tag{3.10}$$

where $n_m = c_m^{\dagger} c_m$ is density operator, V is the n.n. interaction potential. If there are two particles in nearest neighbour sites, interaction potential occurs and second term in Hamiltonian (3.10) checks the sites whether there are neighbour particles or not. This model is also called $t-V$ correlated model. Bloch theorem can be applied as a solution attempt. Fourier transform of operator c_m is know, $c_m = \frac{1}{\sqrt{L}} \sum_k e^{-imk} c_k$. It can be substituted in Hamiltonian (3.10) to quantize system into wave form.

$$\hat{H} = -t \sum_{m} (c_{m+1}^{\dagger} c_m + h.c.) + V \sum_{m} c_m^{\dagger} c_m c_{m+1}^{\dagger} c_{m+1}. \tag{3.11}$$

Lets take interaction term in Hamiltonian into account and apply Fourier transform.

$$\hat{H} = \sum_{k,k',k'',k'''} \frac{1}{\sqrt{L}} e^{imk} c_k^{\dagger} \frac{1}{\sqrt{L}} e^{-imk'} c_{k'} \frac{1}{\sqrt{L}} e^{i(m+1)k''} c_{k''}^{\dagger} \frac{1}{\sqrt{L}} e^{-i(m+1)k'''} c_{k'''}. \tag{3.12}$$

It is known that $c_i c_j^{\dagger} = c_i^{\dagger} c_j = \delta_{c_i, c_j}$. Therefore, $c_k^{\dagger} c_{k'} c_{k''}^{\dagger} c_{k'''}$ term is not zero if $k = k'$, $k' = k''$, $k'' = k'''$. This means $k - k' = k'' - k''' = q$.

$$\hat{H} = \frac{1}{L^2} \sum_{k,k'',q} e^{-iq} c_k^\dagger c_{k-q} c_{k''}^\dagger c_{k''-q}. \tag{3.13}$$

Hamiltonian (3.13) is not diagonal. This means that Hamiltonian (3.10) is not diagonalized by using Bloch theorem. Exact diagonalization method is used to solve this model. Solution method will be given in section 4.2.

3.3 2D lattices

3.3.1 Graphene model with on-site potential

Hexagonal, or honeycomb, lattice is significant for both experimental observations and theoretical calculations. In experiments, it is realised that graphene has hexagonal lattice. Graphene is an allotrope of carbon and it is thinnest two-dimensional material. Many remarkable properties make it very useful and valuable. Same atom arrangement is seen in several other materials. On the other hand, theoretical calculations show many fascinating properties of graphene. Most interesting one is the fact that graphene is semi-metal. Band gaps in the Dirac points may not remain stable when a perturbation is added to system. So, perturbation may not allow system to stay as a semi-metal.

In hexagonal lattice, nearest neighbour vectors are,

$$\delta_1 = a(-1, 0), \quad \delta_2 = a(\frac{1}{2}, -\frac{\sqrt{3}}{2}), \quad \delta_3 = a(\frac{1}{2}, \frac{\sqrt{3}}{2}). \tag{3.14}$$

where a is distance between two sites. Lattice vectors are denoted as a_1 and a_2. Lattice vectors and reciprocal lattice vectors b_i satisfy the identity $b_i \cdot a_j = 2\pi\delta_{i,j}$.

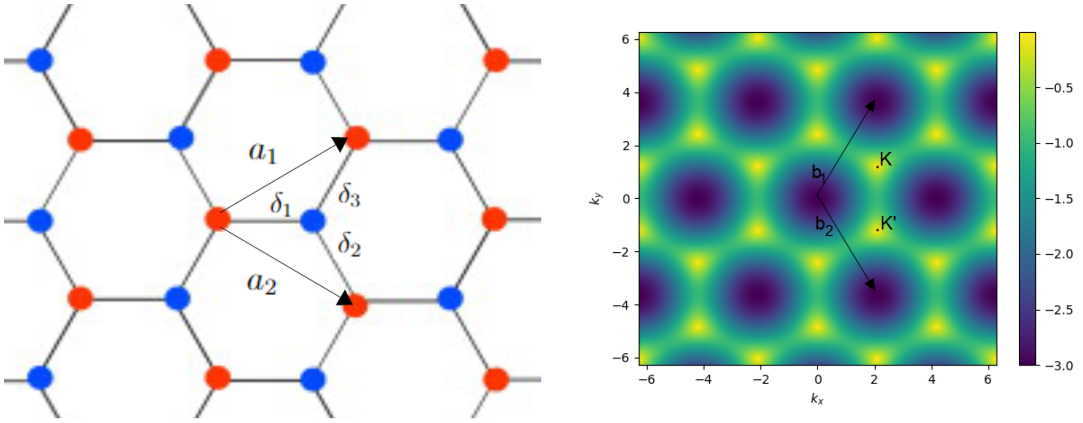

(a) (b)

Figure 3.3: (a) Hexagonal lattice representation with nearest neighbour hopping. Sub-lattice A and sub-lattice B are shown with different colours. (b) Brillouin Zone of hexagonal lattice.

$$a_1 = a(\frac{3}{2}, \frac{\sqrt{3}}{2}), \quad a_2 = a(\frac{3}{2}, -\frac{\sqrt{3}}{2}). \tag{3.15}$$

In this model, n.n hopping and on-site potential are considered. Hamiltonian of this system can be written as,

$$\hat{H} = -J \sum_m (c^\dagger_{B,m} c_{A,m+\delta_1} + c^\dagger_{B,m} c_{A,m+\delta_2} + c^\dagger_{B,m} c_{A,m+\delta_3} + h.c.) \tag{3.16}$$
$$+\Delta \sum_m (c^\dagger_{A,m} c_{A,m} - c^\dagger_{B,m} c_{B,m}).$$

where J are n.n. hopping strength and Δ is on-site potential. $c_{m+\delta}$ annihilates particle on δ neighbour of site m. Nearest neighbours can be written with lattice vector rather than nearest neighbour vectors. Then Hamiltonian in term of lattice vector follows,

$$\hat{H} = -J\sum_m (c^\dagger_{B,m}c_{A,m} + c^\dagger_{B,m}c_{A,m+a_1} + c^\dagger_{B,m}c_{A,m+a_2} + h.c.) \\ +\Delta\sum_m (c^\dagger_{A,m}c_{A,m} - c^\dagger_{B,m}c_{B,m}). \tag{3.17}$$

Bloch states $|\Psi(k)\rangle = |k\rangle \otimes |u(k)\rangle$ can be applied to solve this model as well. Fourier transforms are,

$$c_k = \frac{1}{\sqrt{L}}\sum_m e^{imk}c_m, \qquad c_m = \frac{1}{\sqrt{L}}\sum_k e^{-imk}c_k. \tag{3.18}$$

After substitution Hamiltonian (3.17) becomes,

$$\hat{H} = -J\sum_m\sum_k \left(\frac{e^{-imk}}{\sqrt{L}}c^\dagger_{B,k}\frac{e^{imk}}{\sqrt{L}}c_{A,k} + \frac{e^{-imk}}{\sqrt{L}}c^\dagger_{B,k}\frac{e^{i(m+a_1)k}}{\sqrt{L}}c_{A,k} \right. \\ \left. +\frac{e^{-imk}}{\sqrt{L}}c^\dagger_{B,k}\frac{e^{i(m+a_2)k}}{\sqrt{L}}c_{A,k} + h.c. \right) \\ +\Delta\sum_m\sum_k \left(\frac{e^{-imk}}{\sqrt{L}}c^\dagger_{A,k}\frac{e^{imk}}{\sqrt{L}}c_{A,k} - \frac{e^{-imk}}{\sqrt{L}}c^\dagger_{B,k}\frac{e^{imk}}{\sqrt{L}}c_{B,k} \right). \tag{3.19}$$

It yields,

$$\hat{H} = -J\sum_k (c^\dagger_{B,k}c_{A,k} + e^{ia_1k}c^\dagger_{B,k}c_{A,k} + e^{ia_2k}c^\dagger_{B,k}c_{A,k} + h.c.) \\ +\Delta\sum_k (c^\dagger_{A,k}c_{A,k} - c^\dagger_{B,k}c_{B,k}). \tag{3.20}$$

Matrix form of the Hamiltonian (3.20) follows $\hat{H} = \sum_k c^\dagger_k \hat{h}(k) c_k$ where,

$$\hat{h} = \begin{bmatrix} \Delta & -J(1 + e^{-ika_1} + e^{-ika_2}) \\ -J(1 + e^{ika_1} + e^{ika_2}) & -\Delta \end{bmatrix}. \tag{3.21}$$

d_x, d_y, d_z and d_0 vector of Pauli matrices for this Hamiltonian (3.21) will follow,

$$d_x = -J(1 + \cos(ka_1) + \cos(ka_2)), \qquad d_y = -J(\sin(ka_1) + \sin(ka_2)), \qquad (3.22)$$
$$d_z = \Delta, \qquad d_0 = 0.$$

Hamiltonian (3.17) is reduced to two level Hamiltonian (3.21) in k-space. Eigenvalues within corresponding eigenvectors can be obtained easily. Brillouin zone can be formed by the parallelogram whose edges are b_1 and b_2. There are two symmetry points ,which are denoted as K and K', in that parallelogram and these points form hexagonal Brillouin zone. Around these two points, there are Dirac nodes. Electronic properties stem from those two Dirac points make graphene semi-metal.

3.3.2 Haldane model

Haldane model is an example of topological insulator. It is the first model described as a Chern insulator. Integral of Berry curvature over Brillouin zone is equal to Hall conductance. Filled band gives an integer for Hall conductance and it is called Chern number. Haldane model is described on hexagonal lattice. Next nearest neighbour (n.n.n.) hopping is considered besides on-site potential. This n.n.n. hopping is a complex hooping and it is defined with a hopping strength J' with phase amplitude ϕ. Adding just n.n.n. term with complex hopping to Hamiltonian of the graphane with on-site potential gives the Hamiltonian of the Haldane model.

$$\hat{H}_{Haldane} = \hat{H}_{Graphene} + \hat{H}_{\Delta} + \hat{H}_{NNN}. \qquad (3.23)$$

n.n.n hopping can be taken care of separately for each sub-lattice. Therefore, n.n.n. term can be considered as $\hat{H}_{NNN} = \hat{H}_{NNNA} + \hat{H}_{NNNB}$. Lets take care

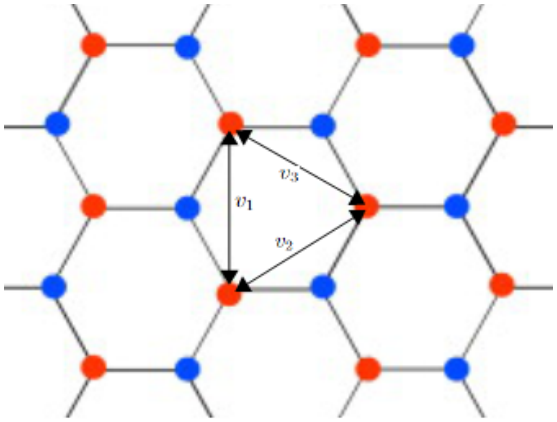

Figure 3.4: Hexagonal lattice representation with next nearest neighbour hopping.

of the n.n.n. hopping for sub-lattice A. In the lattice, next nearest neighbour vectors follows,

$$v_1 = a(\sqrt{3}, 0) \;\; v_2 = a(\frac{\sqrt{3}}{2}, \frac{3}{2}) \;\; v_3 = a(-\frac{\sqrt{3}}{2}, \frac{3}{2}). \tag{3.24}$$

n.n.n. term for sub-lattice A can be written in terms of the n.n.n. vectors as follows,

$$\hat{H}_{NNNA} = -J' e^{i\phi} \sum_m (c^\dagger_{A,m} c_{A,m+v_1} + c^\dagger_{A,m} c_{A,m+v_2} + c^\dagger_{A,m} c_{A,m+v_3}) + h.c. \tag{3.25}$$

By applying Fourier transform of the creation $c^\dagger_m$ and annihilation c_m operators (3.18), Hamiltonian (3.25) yields,

$$\hat{H}_{NNNA} = -J' e^{i\phi} \sum_k (c^\dagger_{A,m} c_{A,k} (e^{ikv_1} + e^{ikv_2} + e^{ikv_3})) + h.c. \tag{3.26}$$

First term of the Hamiltonian (3.26) and its hermitian conjugate basically consist of Euler's formula of the cosine function. Therefore, Hamiltonian (3.26) can be denoted with the cosines functions.

$$\hat{H}_{NNNA} = -2J' \sum_k (\cos(kv_1 - \phi) + \cos(kv_2 - \phi) + \cos(kv_3 - \phi)). \tag{3.27}$$

When creation $c_m^\dagger$ and annihilation c_m operators for sub-lattice A are changed to sub-lattice B and then sign of the complex amplitude ϕ is changed, n.n.n. term for sub-lattice B is obtained.

$$\begin{aligned} \hat{H}_{NNNB} &= \hat{H}_{NNNA}(A \to B \; and \; \phi \to -\phi) \\ &= -2J' \sum_k (\cos(kv_1 + \phi) + \cos(kv_2 + \phi) + \cos(kv_3 + \phi)). \end{aligned} \tag{3.28}$$

So, n.n.n. term in the Hamiltonian is calculated in k-space. n.n. hopping and on-site potential contribution to Hamiltonian have already been calculated in previous section. Adding n.n.n. term to Hamiltonian (3.21) gives the Hamiltonian for Haldane model and its matrix form yields,

$$\hat{H} = \begin{bmatrix} \Delta + H_{NNNA} & -J \sum_k (1 + e^{ika_1} + e^{ika_2}) \\ -J \sum_k (1 + e^{ika_1} + e^{ika_2}) & -\Delta + H_{NNNB} \end{bmatrix}. \tag{3.29}$$

For this two level Hamiltonian (3.29), d_x and d_y vectors did not change. They are same with the d_x and d_y vectors for Graphene. However, d_0 and d_z vector become,

$$d_0 = \frac{H_{NNNA} + H_{NNNB}}{2}, \qquad d_z = \Delta + \frac{H_{NNNA} - H_{NNNB}}{2}. \tag{3.30}$$

or

$$\begin{aligned} d_0 &= -2J' \sum_k \cos(\phi)(\cos(kv_1) + \cos(kv_2) + \cos(kv_3)), \\ d_z &= \Delta - 2J' \sum_k \sin(\phi)(\sin(kv_1) + \sin(kv_2) + \sin(kv_3)). \end{aligned} \tag{3.31}$$

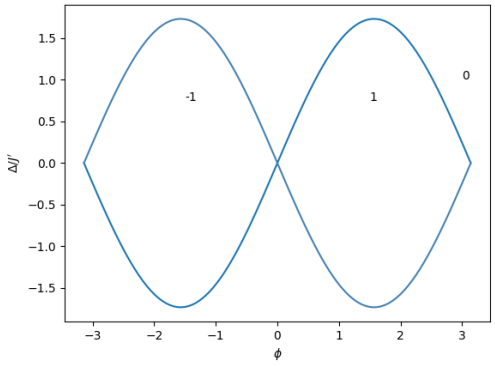

Figure 3.5: Phase diagram of Haldane model. Numbers in the regions are Hall conduction.

If we are on the K or K' points, i.e. $k = K$ or $k = K'$, d_x and d_y would give no contribution as we know from Graphene. However, we would have $d_0 = -3J'\cos(\phi)$ and $d_z = \Delta - \sqrt{3}J'\sin(\phi)$. It is known that energies are $E_\pm = d_0 \pm d$, so energies are $E_\pm = d_0 \pm |d_z|$. These terms affect the gap in the Dirac points. Band gap is equal to,

$$E_+ - E_- = 2|d_z| = 2|\Delta - \sqrt{3}J'\sin(\phi)|. \tag{3.32}$$

Therefore, if Δ is smaller or larger than $\sqrt{3}J'\sin(\phi)$, gap opens in Dirac point and system becomes insulator. For a close gap, Δ is supposed to be equal to $\sqrt{3}J'\sin(\phi)$. This gap-closing case is topological transition point. Hall conductance takes positive or negative integer value when Δ is smaller or bigger than $\sqrt{3}J'\sin(\phi)$. However, Hall conductance become zero and topological transition occurs when $\Delta = \sqrt{3}J'\sin(\phi)$.

Chapter 4

Methods

Definition of localization and polarization are embedded to complex number Z (2.15) in modern theory of polarization. Resta-Sorella showed that polarization is defined by phase of Z [10] and phase is considered the first members of cumulants. It is imposed that x_0 is the center of distribution so that $\int_{-\infty}^{\infty} dx x n_{loc}(x) = 0$. An alternative way to extract cumulants is proposed. This way is based on Z whose phase is removed. Formalism is also extended to two dimensional systems. It was shown that Z depends on system size for specific cases. There are many different scaling laws and among them, idea of renormalization group is taken to consideration to develop another method to observe phase transition point. Besides these definitions, method which is used to solve $t - V$ correlated model is described in this chapter.

4.1 Alternative way to extract cumulants

Extracting cumulants was shown in the chapter 2.3 and equations for cumulants were written. In the way which is proposed to extract cumulants, firstly phase of the Z_q (2.28) is removed.

$$\tilde{Z}_q = Z_q e^{-i \operatorname{Im} \ln Z_q}. \tag{4.1}$$

This approach shifts the distribution in the way where its center becomes zero so that it will be sure that expansion to obtain cumulants is always around zero. $\tilde{Z}_q$ always contains the minimum error terms. In the next step, $\tilde{Z}_q$ is substituted into equation (2.20) but before that finite difference approximation is applied. For instance, consider cumulant generating function (2.31) with characteristic function (4.1) where order n is two and four.

$$\begin{aligned} \tilde{C}_2 &= \left(\frac{L}{2\pi i}\right)^2 [\ln \tilde{Z}_q]^{(2)}_{q=0}, \\ \tilde{C}_4 &= \left(\frac{L}{2\pi i}\right)^4 [\ln \tilde{Z}_q]^{(4)}_{q=0}. \end{aligned} \tag{4.2}$$

Equations (4.2) give the second and fourth cumulants. When finite difference approximation is applied, second and fourth cumulants can be written as follows,

$$\begin{aligned} \tilde{C}_2^{(1)} &= \left(\frac{L}{2\pi i}\right)^2 (\tilde{Z}_1 - 2\tilde{Z}_0 + \tilde{Z}_{-1}), \\ \tilde{C}_2^{(2)} &= \left(\frac{L}{2\pi i}\right)^2 \frac{(-\tilde{Z}_2 + 16\tilde{Z}_1 - 30\tilde{Z}_0 + 16\tilde{Z}_{-1} - \tilde{Z}_{-2})}{12}. \end{aligned} \tag{4.3}$$

$$\begin{aligned} \tilde{C}_4^{(1)} &= \left(\frac{L}{2\pi i}\right)^4 (\tilde{Z}_2 - 4\tilde{Z}_1 + 6\tilde{Z}_0 - 4\tilde{Z}_{-1} + \tilde{Z}_{-2}), \\ \tilde{C}_4^{(2)} &= \left(\frac{L}{2\pi i}\right)^4 \frac{(-\tilde{Z}_3 + 12\tilde{Z}_2 - 39\tilde{Z}_1 + 56\tilde{Z}_0 - 39\tilde{Z}_{-1} + 12\tilde{Z}_{-2} - \tilde{Z}_{-3})}{6}. \end{aligned} \tag{4.4}$$

The superscript in parentheses refers to lowest (C^1) and second lowest (C^2) order accuracy of the finite difference approximation. Z_0 is just a normalization

so it is equal to one. Moreover, Z_q and Z_{-q} are equal to each other because they have the same closed path. Then, second and fourth cumulants with first two lowest order finite difference approximation follow as;

$$\tilde{C}_2^{(1)} = \left(\frac{L}{2\pi i}\right)^2 2(\tilde{Z}_1 - 1), \tag{4.5}$$
$$\tilde{C}_2^{(2)} = \left(\frac{L}{2\pi i}\right)^2 \frac{(-\tilde{Z}_2 + 16\tilde{Z}_1 - 15)}{6}.$$

$$\tilde{C}_4^{(1)} = \left(\frac{L}{2\pi i}\right)^4 2(\tilde{Z}_2 - 4\tilde{Z}_1 + 3), \tag{4.6}$$
$$\tilde{C}_4^{(2)} = \left(\frac{L}{2\pi i}\right)^4 \frac{(-\tilde{Z}_3 + 12\tilde{Z}_2 - 39\tilde{Z}_1 + 28)}{3}.$$

In the case of extreme localization, Z_q values would take zero value except Z_0 which is always equal to one. So that, when we have an ideal conductor, mth cumulant will be proportional to $\left(\frac{L}{2\pi i}\right)^m$. Only error term would affect the cumulants calculations. Result of cumulants calculation depends on a coefficient provided by order of finite difference approximation n. In ideal conductor case, the second cumulant (variance) will be in the form,

$$C_2^{(n)} = A_n \frac{L^2}{4\pi^2}. \tag{4.7}$$

Main difference between alternative cumulant expression and the Resta-Sorella expression is the error terms which they contain. When we substitute characteristic function into Resta-Sorella's second cumulant expression, we obtain,

$$\left(\frac{L}{2\pi i}\right)^2 2\,\mathrm{Re}\ln Z_1 = C_2 + \left(\frac{2\pi i}{L}\right)^2 \frac{C_4}{12} + \mathcal{O}(L^{-4}). \tag{4.8}$$

Cumulant	Order	$\tilde{Z}_0$	$\tilde{Z}_1$	$\tilde{Z}_2$	$\tilde{Z}_3$	$\tilde{Z}_4$
$\tilde{C}_2$	1	-2	2			
	2	-5/2	8/3	-1/6		
	3	-49/18	3	-3/10	1/45	
	4	-205/72	16/5	-2/5	16/315	-1/280
$\tilde{C}_4$	1	6	-8	2		
	2	28/3	-13	4	-1/3	
	3	91/8	-244/15	169/30	-4/5	7/120
$\tilde{C}_6$	1	-20	30	-12	2	
	2	-75/2	58	-26	6	-1/2

Table 4.1: Table contains the coefficients of polarization amplitudes for few cumulants up to several orders. They are equivalent to coefficients of the central finite differences.

On the other hand, alternative way to express second cumulant yields,

$$\left(\frac{L}{2\pi i}\right)^2 2(\tilde{Z}_1 - 1) = C_2 + \left(\frac{2\pi i}{L}\right)^2 \frac{C_4}{12} + \left(\frac{2\pi i}{L}\right)^2 \frac{C_2^2}{4} + \mathcal{O}(L^{-4}). \tag{4.9}$$

In the appendix A, detailed calculations are given. It is expected that cumultans extracted with alternative way give finite size scaling exponent two for an ideal conductor like Resta-Sorella's expression. However, when we compare the equation (4.8) and equation (4.9), it is seen that cumulants are extracted with alternative way have additional error terms. Therefore, it is expected that results more accurate with alternative way because of this contributions.

4.2 Exact diagonalization for t-V model

As it is discussed in chapter 3.2, Hamiltonian of the t-V model follows as,

$$\hat{H} = J \sum_m (c_{m+1}^\dagger c_m + h.c.) + V \sum_m n_m^\dagger n_{m+1}. \tag{4.10}$$

When Bloch theorem is used, Hamiltonian (3.13) is received and it is not diagonal. It is not possible to use Bloch state and solve Hamiltonian with tight binding model. So that, Hamiltonian is solved with exact diagonalization. Since operator c_m annihilates a particle on site m while $c_m^\dagger$ creates particle on site $m+1$, first part of the Hamiltonian has basis set $\{|m_i\rangle\}$. On the other hand, since operator n_m is density function on site m, second part of the Hamiltonian has basis set $\{|l_i\rangle = |m_1, m_2, m_3, ..., m_L\rangle\}$. These two parts are written in same basis set. Then, Hamiltonian is constructed and eigenvalues with corresponding eigenvectors are obtained from the Hamiltonian by diagonalizing it. Firstly, first part in the Hamiltonian is written in term of the basis set of the second part. Then, two parts are combined and Hamiltonian is constructed in one basis.

As an example, suppose that $L = 4$ and $N = 2$ then $\{|m\rangle\}$ has four basis vector i.e. $\{|m_1\rangle, |m_2\rangle, |m_3\rangle, |m_4\rangle\}$ and each basis vector represents empty $|0\rangle$ or filled $|1\rangle$ site. Number of basis vector of $\{|l\rangle = |m_1, m_2, m_3, m_4\rangle\}$ depends on combination of filling $\{|m\rangle\}$. Number of all combination is calculated by $\frac{L!}{(L-N)!N!}$ so in this example it has six basis vectors. In binary representation, it follows as,

$$\{|1,1,0,0\rangle,\ |1,0,1,0\rangle,\ |1,0,0,1\rangle,\ |0,1,1,0\rangle,\ |0,1,0,1\rangle,\ |0,0,1,1\rangle\} \tag{4.11}$$

Matrix form of the Hamiltonian is written with second part's basis set as follows,

$$\hat{H}_{ED} = \begin{bmatrix} \langle l_1|\hat{H}|l_1\rangle & \langle l_1|\hat{H}|l_2\rangle & \langle l_1|\hat{H}|l_3\rangle & \cdots & \cdots \\ \langle l_2|\hat{H}|l_1\rangle & \langle l_2|\hat{H}|l_2\rangle & \langle l_2|\hat{H}|l_3\rangle & \cdots & \cdots \\ \langle l_3|\hat{H}|l_1\rangle & \langle l_3|\hat{H}|l_2\rangle & \langle l_3|\hat{H}|l_3\rangle & \cdots & \cdots \\ \vdots & \vdots & \vdots & \ddots & \\ \vdots & \vdots & \vdots & & \ddots \end{bmatrix}. \tag{4.12}$$

Therefore, matrix form of the Hamiltonian becomes,

$$\hat{H} = \begin{bmatrix} 0 & J & 0 & 0 & J & 0 \\ J & 0 & J & J & 0 & J \\ 0 & J & 0 & 0 & J & 0 \\ 0 & J & 0 & 0 & J & 0 \\ J & 0 & J & J & 0 & J \\ 0 & J & 0 & 0 & J & 0 \end{bmatrix} + \begin{bmatrix} V & 0 & 0 & 0 & 0 & 0 \\ 0 & 0 & 0 & 0 & 0 & 0 \\ 0 & 0 & V & 0 & 0 & 0 \\ 0 & 0 & 0 & V & 0 & 0 \\ 0 & 0 & 0 & 0 & 0 & 0 \\ 0 & 0 & 0 & 0 & 0 & V \end{bmatrix} = \begin{bmatrix} V & J & 0 & 0 & J & 0 \\ J & 0 & J & J & 0 & J \\ 0 & J & V & 0 & J & 0 \\ 0 & J & 0 & V & J & 0 \\ J & 0 & J & J & 0 & J \\ 0 & J & 0 & 0 & J & V \end{bmatrix}. \tag{4.13}$$

Ground state energy and its vector of this matrix are found. During computational calculations, linear algebra package may be used and ground state energy with its vector can be obtained with help of functions provided by package. However, direct methods are not practical to use. Increase in the system size of the system cause huge dimensions in matrix of the Hamiltonian. therefore, the required computational storage significantly increased a lot. In the above example, basis set has $\frac{4!}{(4-2)!2!} = 6$ elements so Hamiltonian matrix is 6-by-6. Suppose that, system size L is 24 and it is half filled then dimension is $\frac{24!}{(24-12)!12!} = 2704156$. It is impossible to solve such a matrix. Lanczos algorithm is used to overcome this problem.

4.3 Lanczos algorithm

Usual eigenvalue problems are about computing smallest/largest eigenvalues, along with corresponding eigenvectors. Direct methods are hard to use to obtain eigenvalues and eigenvectors of large matrices. Lanczos algorithm is an iterative method to find such eigenvalues and their eigenvectors of large matrices. It gives good approximate answers with far less storage than direct methods.

Assume that the problem is to find largest eigenvalue of matrix A and it's eigenvector. Power method can be used to find them by starting with given vector x. Inner loop follows as $y_{i+1} = Ax_i$, $x_{i+1} = y_{i+1}/|y_{i+1}|$. The vector x converges to the expected eigenvector. Besides, problem can be finding the

closest eigenvalue to λ. This problem is similar to previous one. Result of this problem can be approximated with inverse iteration. This inner loop follows as $y_{i+1} = (A - \lambda I)^{-1} x_i$, $x_{i+1} = y_{i+1}/|y_{i+1}|$. In this case, vector x converges as well. With start with the given vector x, both methods create vector sequence such as $\{x_1, x_2, x_3, ..., x_k\}$. These vectors span the Krylov subspace. Instead of taking vector x_k in the vector sequence as a approximated desired eigenvector, best approximated vector in Krylov subspace can be focused. Best linear combination of the vectors which span the Krylov subspace gives much better approximated eigenvector then the x_k. Eigenvalue of this eigenvector can be approximated by Rayleigh-Ritz method by eigenvalue of matrix T where $T = Q^T AQ$. This best approximated result is called Ritz value. Theorems, proofs etc. which justifies that Ritz value is the eigenvalue approximation are not given in this section. Reader can check the [29] for more detailed descriptions.

For symmetric matrix A, Lanczos algorithm combines building Krylov subspace and Rayleigh-Ritz procedure to find eigenvalues along with corresponding eigenvectors. Convergence gives reliable result. With k iteration, Lanczos vectors q construct an orthogonal matrix $Q_k = [q_1, q_2, ..., q_k]$ and eigenvalues of A are approximated by a eigenvalues of the symmetric triangular matrix $T_k = Q_k^T A Q_k$. With given vector $|v_0\rangle$ of length n, this algorithm follows the following steps;

$$
\begin{aligned}
q_1 = v_0/|v_0|, \quad \beta_0 = 0, \quad q_0 = 0 \\
\text{for } i = 1 \text{ to } k \\
w = Aq_i \\
\alpha_j = w^T q_j \\
w = w - \alpha_i q_i - \beta_{i-1} q_{i-1} \\
\beta_i = |w| \\
\text{if} \beta_i = 0, \text{ quit} \\
q_{i+1} = w/\beta_i
\end{aligned}
\tag{4.14}
$$

Vectors q_i produce matrix Q n-by-k and matrix T k-by-k is constructed as

$$T = \begin{bmatrix} \alpha_1 & \beta_1 & & \\ \beta_1 & \ddots & \ddots & \\ & \ddots & \ddots & \beta_{k-1} \\ & & \beta_{k-1} & \alpha_k \end{bmatrix}. \tag{4.15}$$

Eigenvalue e of the matrix T is the best approximated eigenvalue of the matrix A. Corresponding eigenvector v_e of eigenvalue e plays role to obtain best linear combination of the vectors q. Following Linear combination, gives the best approximated eigenvector $|v\rangle$ of the matrix A for the corresponding eigenvalue.

$$|v\rangle = \sum_k v_e(k) q_k. \tag{4.16}$$

Result for the smallest/largest eigenvalues, along with corresponding eigenvectors converge very fast. Convergence slows down as obtaining the results far from the smallest/largest values. Even if Lanczos algorithm requires much less storage then the direct methods, Matrix A can be too huge so that it won't be possible to save matrix Q. In such case, Lanczos algorithm can be applied two times. In first Lanczos run is used to construct matrix T and obtain eigenvalue with its eigenvector from matrix T. Because matrix T is k-by-k , not like matrix Q n-by-k, it is possible to save it. Then with second Lanczos run, obtained eigenvector from matrix T can be used for linear combination of vectors q inside the loop.

4.4 Renormalization Group

Many different scaling laws exist and several of them have been very common throughout ages. One of the scaling argument is renormalization group and it was developed to scale transformations in quantum electrodynamics [25, 26]. It is discovered that coupling parameter g with scale n can be written with group equation G as,

$$g(n) = G^{-1}(\left(\frac{n}{m}\right)^{\alpha} G(g(m))). \tag{4.17}$$

where α is a constant. It follows,

$$G(g(n)) = \left(\frac{n}{m}\right)^{\alpha} G(g(m)). \tag{4.18}$$

Coupling parameter g in scale n is written in terms of coupling parameter g in scale m but another it could be written in different scale. This transformation continues with infinitesimally small changes in scales and a flow equation was obtained. Stemming from this equation, renormalization group equation was reached.

$$\psi(g) = \beta(g). \tag{4.19}$$

It is also called beta function. Leo P. Kadanoff proposed the "block-spin" renormalization group [30]. It is one of the simple ways for a better understanding renormalization group. Consider a block which contains correlated spins. It could be 2D Ising model. Hamiltonian H will be in term of spins σ in each cell. For large systems, considering all spins and correlations are not easy way to reach a result. Some transformations can simplify the system. For instance, forming spins with new scale may reduce the degree of freedom. Critical points which do not rely on the degree of freedom will not be affected. Firstly, spins are divided to groups. For example, four nearest spins can be grouped in 2D block system. Each group's spins is renormalized and new block is formed. Then new spin block Hamiltonian H' will be in term of spins σ'. This scaled Hamiltonian H' will be related Hamiltonian H with a renormalization constant.

$$H(\sigma) = R^{\alpha} H'(\sigma'). \tag{4.20}$$

This iteration can be done again and again. After enough iteration, the critical point is reached.

$$H_{critical}(\sigma) \simeq H^{'}_{critical}(\sigma^{'}) = H^{*}. \tag{4.21}$$

Under this idea, critical point where correlated system has phase transition is estimated. Polarization amplitude $Z(L, V)$ is renormalized by $L/2$ scale. Where L is the system size and V is the correlation potential.

$$Z(L, V) = R^{\alpha} Z(L/2, V^{'}). \tag{4.22}$$

After enough iteration, these equivalence of these polarization amplitude is obtained. This correlated potential V which induced that equivalence is regarded as critical point where phase transition occur.

$$Z(L, V_{critical}) = Z(L/2, V_{critical}) = Z^{*}. \tag{4.23}$$

4.5 Two Dimensional Amplitude

This approach is based on the regarding polarization as one dimensional vector quantity. Therefore, two dimensional models are reduced to one dimensional sub-models to investigate. The equation (2.29) is used to calculate Z_q with following form,

$$Z_q = \langle \Psi(r) | e^{i(2\pi q/L)\hat{R})} | \Psi(r) \rangle. \tag{4.24}$$

Vector r is direction of the polarization and $\hat{R}$ is the position operator along this direction. The paths which an electron can follow are considered the direction of the polarization. Then phase calculations are done over these directions. In the graphene with nearest neighbour hopping, there are three neighbour vector as shown in equation (3.14). Therefore, it is considered that there are three paths. As it is shown in the section 3.3.1, graphene model is solved with tight binding model. As well as lattice vectors a_1 and a_2 is converted to reciprocal lattice vectors b_1 and b_2 in the k-space, neighbour vector is also converted to,

$$\zeta_1 = \frac{4\pi}{3\sqrt{3}}(0,1) \;\; \zeta_2 = \frac{4\pi}{3\sqrt{3}}(\frac{\sqrt{3}}{2}, -\frac{1}{2}) \;\; \zeta_3 = \frac{4\pi}{3\sqrt{3}}(-\frac{\sqrt{3}}{2}, -\frac{1}{2}). \tag{4.25}$$

In the Brillouin zone, a path which follows any of these directions comes across the Dirac points. This one dimensional sub-model becomes very similar to the SSH model. Therefore, it is expected that results give size scaling exponents two, geometric Binder cumulants 0.5 and other properties for an ideal conductor. Deviating from one of these paths cause distortion on results. Consider a path which doesn't follow the direction to nearest neighbour and follows the direction to next nearest neighbour, i.e., one of the directions described in equation (4.25). Even if that path also comes across the Dirac points, expected results for an ideal conductor are not received. Adding next nearest neighbour hopping to Hamiltonian eliminates the distortion on results obtained by this path. Adding hopping between sites creates new paths which electrons can follow so that paths which follow the direction between these two sites gives the expected results as well.

Above approach is not sufficient to investigate all models. When Dirac nodes from a line in Brillouin zone rather than points, it is not possible to reduce the two dimensional model to one dimensional sub-model similar to SSH model. Shifting the path, without changing the direction, cause not a random distortion. Results is deflected by following a behaviour. This behaviour means something. By regarding that, this one dimensional calculations is extended to two dimensional calculations. Polarization amplitude is calculated over nth Brillouin zone. Polarization calculation is started with a path described above. Then, path is shifted so that all nth Brillouin zone is covered. Polarization amplitude described can

be written as,

$$Z_q = \langle \Psi(r_x, r_y) | e^{i(2\pi q/L)\hat{R}_y} | \Psi(r_x, r_y) \rangle = \prod_{nthBZ} \langle r_x, r_y | | r_x, r_y + q \rangle. \tag{4.26}$$

where r_y is the direction of the path and r_x is the direction of the shift. While system has nth nearest neighbour hopping, nth Brillouin zone is considered. With this approach, whole nth Brillouin zone contribute to the polarization amplitude calculation. This contribution improves the results and makes the formalism valid for two dimensional models which have Dirac points or Dirac nodes.

Chapter 5

Results

For the ideal conductor case, second cumulant (variance) is equal to the coefficient A_n, which depends on order of the finite difference approximation (n), times the L^n. Increase in the order n causes an increase in coefficient A_n. That change converges to an upper bound as a function of n. It is estimated that this upper bound which A_n converges is 3.224. For ideal conductor case, geometric Binder cumulant is 0.5 as we expected but there is a reduction in value of Geometric Binder cumulant. This shows that increase in the coefficient A_n cause less correction in the calculation of the geometric Binder cumulant and higher orders of the finite difference approximation distort the expected values for the ideal conductor case.

Resta-Sorella's definition shows the difference between insulating and metallic states. For metallic case, phase is independent from system size L so that second cumulant only depends on the second exponent of the system size. When on site potential is added, phase transition occurs. In insulating case, phase becomes dependent to system size and second cumulant exponent is one. Same behaviour is obtained by alternative way to extract cumulants which is proposed, see figure (5.2). However, with Resta-Serolla's definition, figure (5.2.a), size scaling exponent exceeds the lower bound after the phase transition and then get back to it. When new formalism with finite difference approximation with lowest order

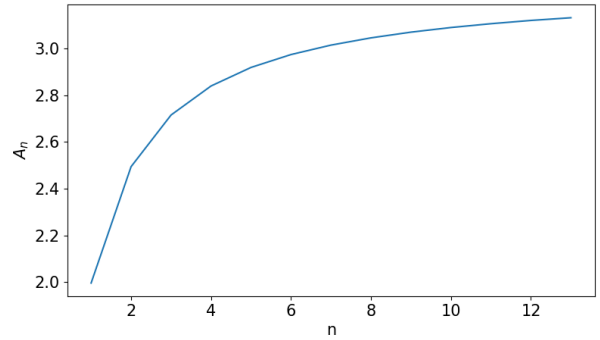

(a)

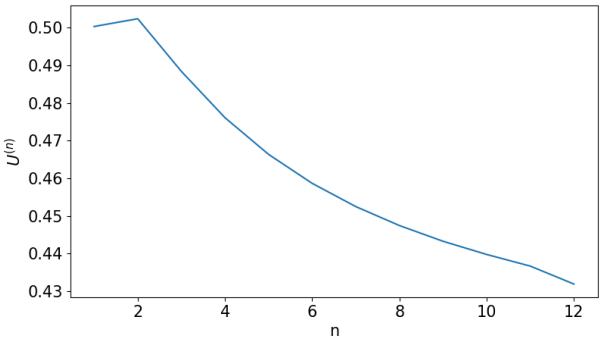

(b)

Figure 5.1: Upper panel shows coefficient A_n and lower panel shows Geometric Binder Cumulant under the change of the order of the finite difference approximation in the ideal conductor case.

accuracy is applied, figure (5.2.b), that exceeding the lower bound is substantially reduced. After the phase transition, size scaling exponent hardly exceed the lower bound. Moreover, size scaling exponent goes to one more smoothly during transition from metallic case to insulating state. With finite difference approximation with second order accuracy, figure (5.2.c), behaviour of size scaling exponent is very similar with the results obtained by Resta-Sorella's definiton.

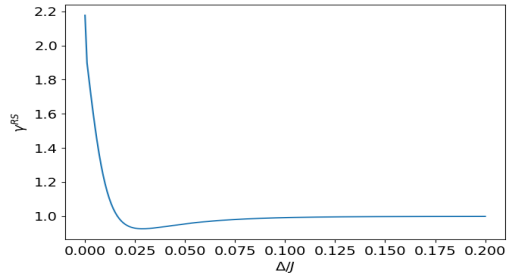

(a)

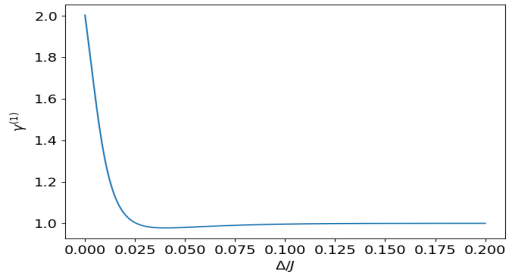

(b)

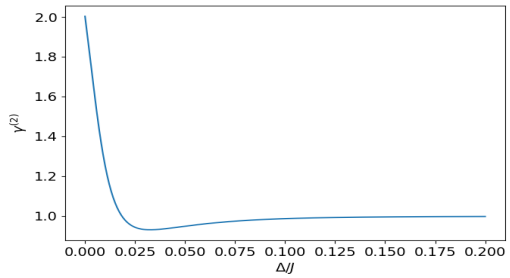

(c)

Figure 5.2: Size scaling exponent γ for SSH model. (a) cumulants are obtained by Resta-Sorella definition. (b) and (c), cumulants are obtained by alternative way proposed. The superscript in parentheses refers order of accuracy of the finite difference approximation. Size scaling exponent is calculated with system sizes $L =$. n.n. hopping strength is set to 1.

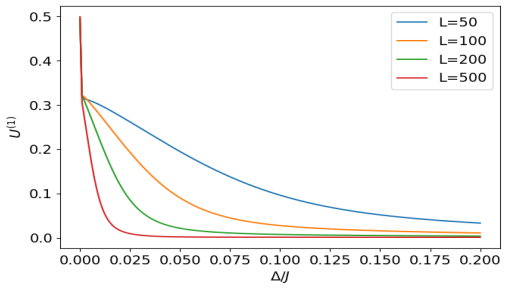

(a)

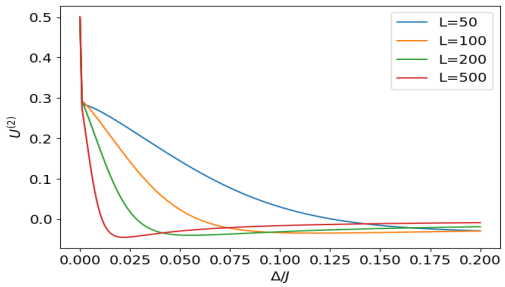

(b)

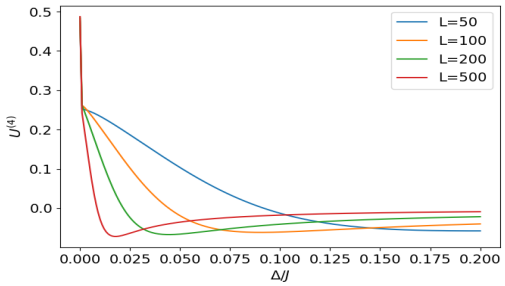

(c)

Figure 5.3: Geometric Binder Cumulant (U) for SSH model. Cumulants by finite difference approximation with (a), first order, (b) second order, (c) third order. n.n. hopping strength is set to 1.

Geometric Binder cumulant (GBC) shows the difference between insulating and metallic states just like size scaling exponent, see figure (5.3). When there is no impurity and system is in metallic case, ratio of second and fourth cumulants gives constant value and GBC take the value 0.5. When on-site potential added, system becomes an insulator case and ratio of cumulants goes to 0. Therefore, GBC reaches to lower bound 0 for insulating case. That transition is affected by system size. When system size is larger, GBC goes from 0.5 to 0 after phase transition more sharply. With first order finite difference approximation, GBC does not exceed the lower bound, figure (5.3.a). With second order finite difference approximation, GBC exceeds the lower bound after phase transition and then get back to it, figure (5.3.b). This aberration is larger when order of finite difference approximation is increased, figure (5.3.c).

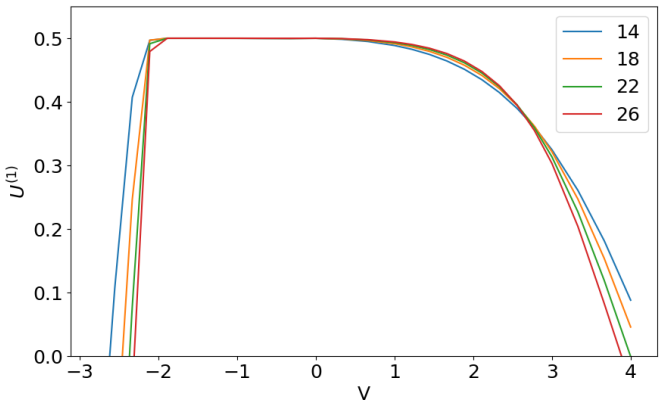

(a)

Figure 5.4: Geometric Binder cumulant for t-V correlated model. interaction. Hopping strength is set to 1.

System Sizes	Fixed Points	Fixed Points
L = 16-8	V = 3.00	V = -2.21
L = 20-10	V = 2.75	V = -2.13
L = 24-12	V = 2.62	V = -2.08
L = 28-14	V = 2.52	V = -2.06

Table 5.1: Critical n.n interaction potential V values which satisfies the equation (4.20) for SSH model with n.n. interaction.

We can also observe the phase transition between metallic case and insulating case for t-V correlated model. GBC follows the upper bound 0.5 until phase transition occurs. Transition is much more sharp when n.n. interaction is repulsive (-V) comparing to attractive potential (V), figure (5.4). For repulsive potential, GBC suddenly reduces from the value 0.5 at the point very close to 2.00 so that phase transition point is almost $2J$. However, for the attractive potential, it is difficult to locate transition point and it is around $2.5J$. By using the renormalization group method, critical n.n. interaction potential which satisfies the equation (4.20) is found, see table (5.1). This fixed points represent the phase transition point. With larger system sizes, fixed points converges and it is good agreement with the GBC results.

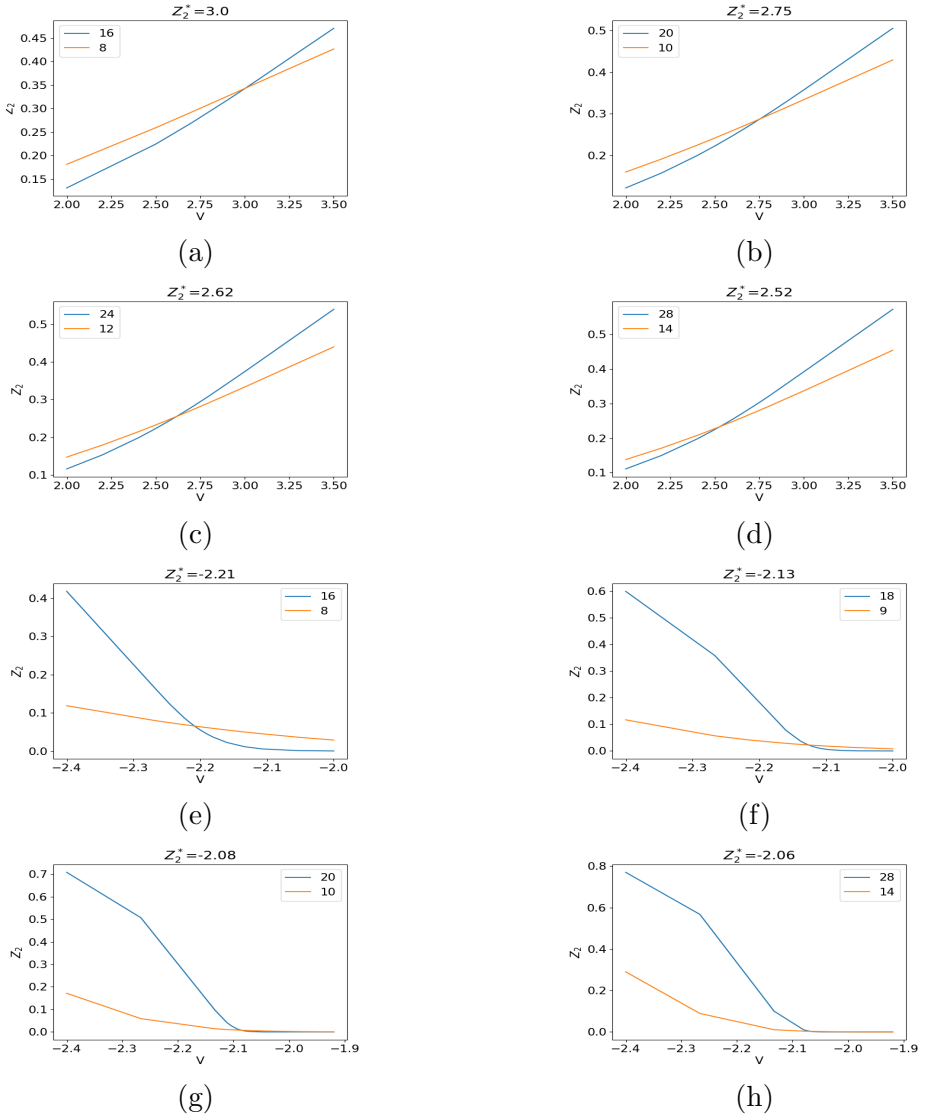

Figure 5.5: Z_2 values for SSH model with n.n. interaction (t-V correlated model). Each plot contains data for a L and $L/2$ variables to obtain critical Z^* values which renormalization group theory suggests.

Two dimensional model graphane is reduced to one-dimensional sub-lattice and GBC is calculated with this approach. In figure (5.6.b), GBC is calculated with the path over n.n. direction ζ_1 in equation (4.22). There is no impurities, so system is in metallic case and GBC value is 0.5. Calculation is shifted by direction which is perpendicular to the direction where phase is calculated. In figure (5.6.b) calculation, it is k_x direction. Change of k_x value distort the GBC value. On the other hand, we can change path where GBC is calculated by changing the direction. In figure (5.6.d), calculations are done over path in different nth neighbour directions. Path over n.n. direction gives the 0.5 GBC value however GBC value is again distorted for path over other nth neighbour directions.

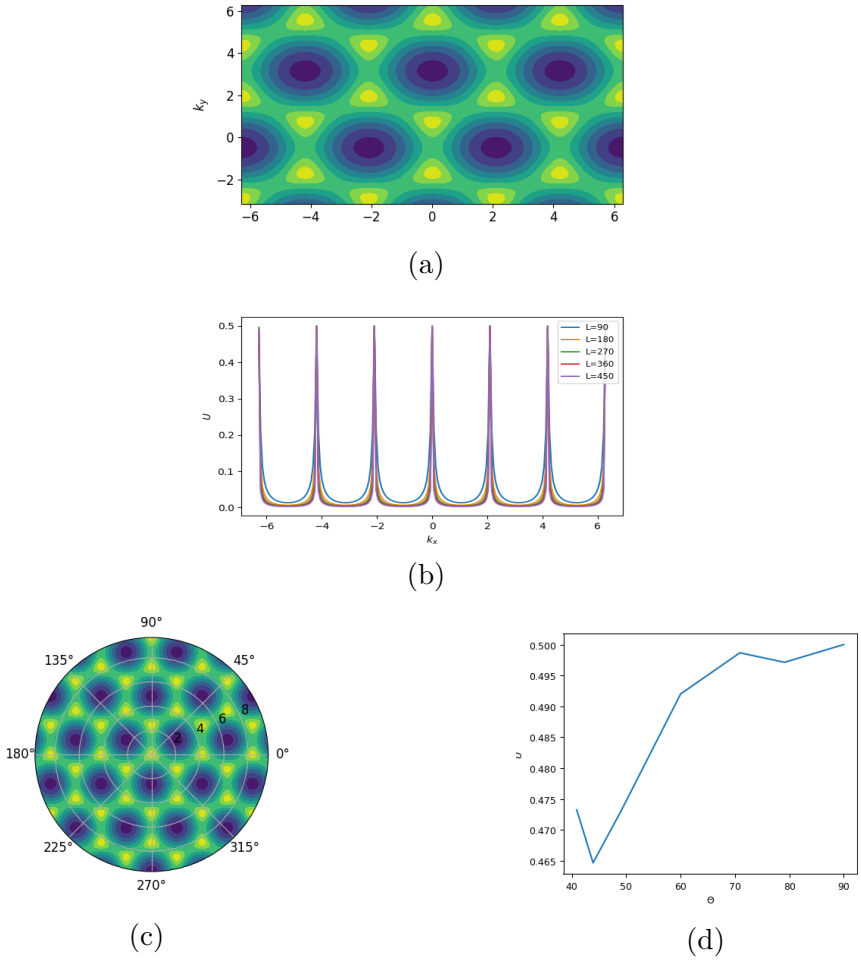

(a)

(b)

(c)

(d)

Figure 5.6: Geometric Binder cumulants for one dimensional sub-models of graphene. (b) Paths is shifted over Brillouin zone. (d) Path is rotated and calculation is done for nth nearest neighbours.

GBC calculation is done with same approach under the change of the on-site potential V. GBC is 0.5 when there is no on-site potential as it is expected for ideal conductor case. When on-site potential is added, GBC changes. It goes to lower bound 0 under the increase of the on site potential, see figure (5.7). Size dependency is apparent where graphene is affected by on site potential. After phase transition occurs, GBC reach to lower bound 0 much more suddenly. GBC is also calculated for Haldane model. When Haldane model has ideal conductor case i.e. $|\Delta| = |\sqrt{3}J' \sin(\phi)|$, GBC takes the value of 0.5. Rather than this conditions, GBC dramatically reduces to the lower bound 0, see figure (5.8.a). Similar to the graphene, size dependency is apparent while this condition is not satisfied and GBC reach to lower bound 0 much more suddenly when phase transition occurs, see figure (5.8.b).

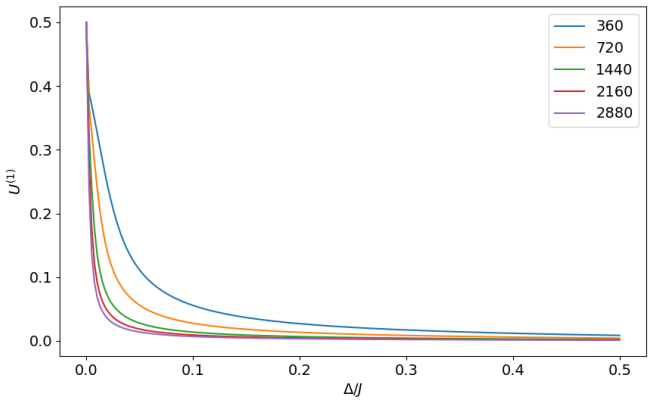

(a)

Figure 5.7: GBC for hexagonal lattice with on site potential. n.n. hopping strength set to 1.

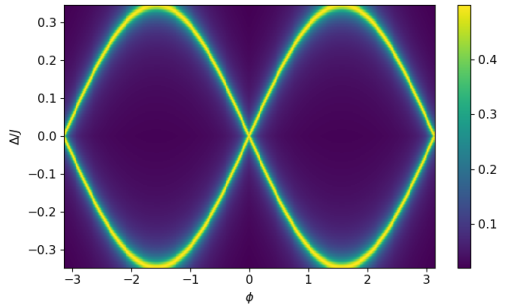

(a)

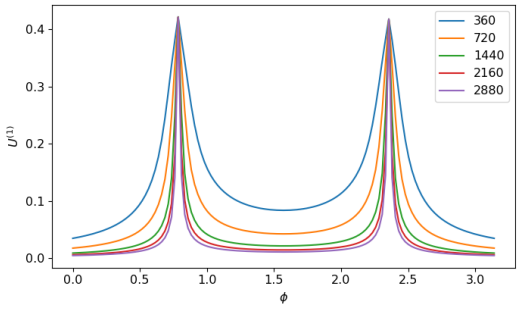

(b)

Figure 5.8: Geometric Binder cumulant for Haldane model. n.n. hopping strength is set to 1 and n.n.n. hopping strength is set to 0.2.

In figure (5.9), GBC calculations are done over Brillouin zone. This allows us to investigate square lattice whose Fermi surface is Dirac nodes like other investigated models which have Dirac points. GBC shows similar behavior compared to Graphene. GBC takes the value 0.5 for ideal conductor case and it reduces to lower bound 0 when system is affected by on site potential. However, transition point does not occur immediately just after impurity is added. Phase transition is at approximately at 0.034. Figure (5.9.b) show the same behavior of GBC for Graphene where we can see in figure (5.7). Again, we have 0.5 GBC value for ideal conductor case and it reduces to lower bound 0 when system is affected by on site potential. We can also see the size dependency where there is impurity in the system. However, it is more sensitive to system size. GBC requires more high system size to suddenly reach to lower bound after phase transition. For Haldane model, expected behavior is obtained but strong size dependency can be seen in the results. GBC takes the value 0.5 for conductor case but requires high system size to suddenly reach lower bond 0.5 after phase transition.

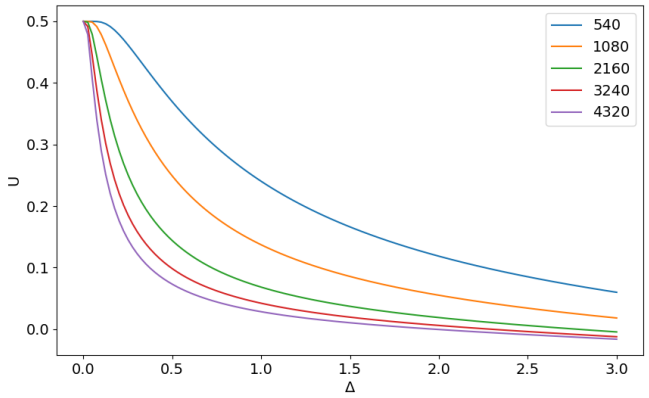

(a)

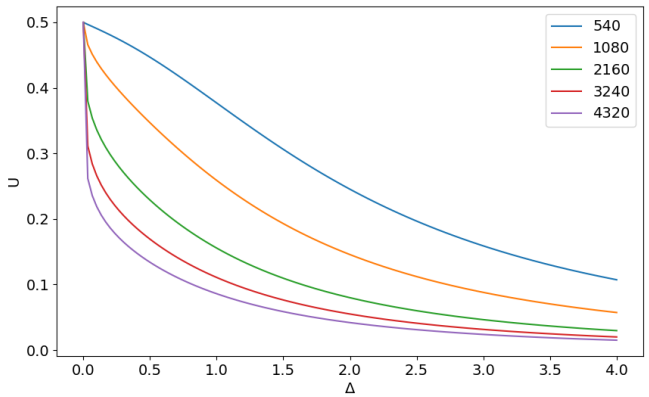

(b)

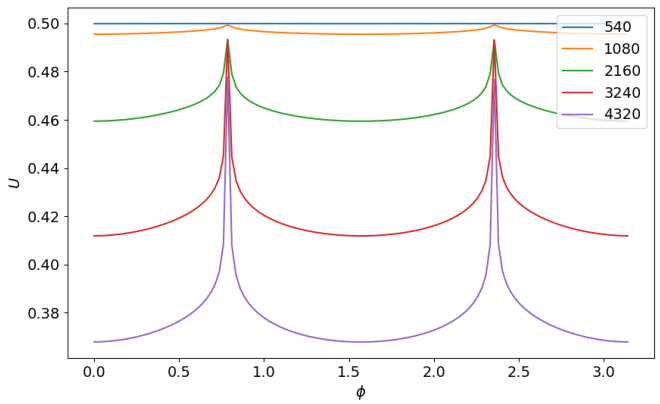

(c)

Figure 5.9: Geometric Binder cumulants calculated over Brilioun zone for two dimensional models. (a) Square model, (b) Graphene model, (c) Haldane model.

Chapter 6

Conclusion

One can obtain gauge invariant cumulants based on geometric phase. An alternative way is proposed to extract cumulants associated adiabatic cycle and this way adds corrections to the error terms. It was shown that a geometric quantity is reached by ratio of these cumulants with a particular way. A well defined geometric quantity associated with adiabatic cycle is constructed.

This alternative way is tested and compared with Resta-Sorella's definition. Cumulants and geometric quantities constructed by these cumulants depends on the order of the finite difference approximation. Results obtained from Resta-Sorella's definition are very similar to results obtained by alternative way with second order finite difference approximation. Results obtained by alternative way with first order finite difference approximation is a little bit more sensitive difference between gap closure and show transition between conductor case and insulator case. Moreover, it eliminates the most of the distortion in the results around transition point. Geometric Binder cumulant ,which is constructed with cumulants extracted by alternative way, is investigated as a quantity used in the context of modern theory of polarization. It is shown that geometric Binder cumulants also procedure size scaling relations. It is size independent at gap closure otherwise shows size dependent behavior. However, in order to observe insulating

or conductor cases, geometric Binder cumulant does not need size scaling exponent. Geometric Binder cumulants shows the transition between these two cases and have much less distortion around phase transition point compared to size scaling exponent. Increasing system size improves the observation. Formalism is developed to also observe two dimensional systems. It is shown that it is possible to calculate a geometric quantity which is sensitive to whether a given system is gapped or not. Geometric Binder cumulants which is calculated for two dimensional systems provides the phase transition between metallic and insulator case. Moreover, this quantity allows us to investigate the systems whose Fermi surface is one or zero dimensional. For comparison, another method based on renormalization group theory is used to locate phase transition. Determined fix points converges to a value and it is in good agreement with phase transition point which are provided by Geometric Binder cumulant.

Bibliography

[1] M. V. Berry, "Quantal phase factors accompanying adiabatic changes," *Proceedings of the Royal Society of London. A. Mathematical and Physical Sciences*, vol. 392, no. 1802, pp. 45–57, 1984.

[2] J. Zak, "Berry's phase for energy bands in solids," *Physical review letters*, vol. 62, no. 23, p. 2747, 1989.

[3] B. A. Bernevig, "Topological insulators and topological superconductors," in *Topological Insulators and Topological Superconductors*, Princeton university press, 2013.

[4] M. Franz and L. Molenkamp, *Topological insulators*. Elsevier, 2013.

[5] C. L. Kane and E. J. Mele, "Quantum spin hall effect in graphene," *Physical review letters*, vol. 95, no. 22, p. 226801, 2005.

[6] C. L. Kane and E. J. Mele, "Z 2 topological order and the quantum spin hall effect," *Physical review letters*, vol. 95, no. 14, p. 146802, 2005.

[7] F. D. M. Haldane, "Model for a quantum hall effect without landau levels: Condensed-matter realization of the" parity anomaly"," *Physical review letters*, vol. 61, no. 18, p. 2015, 1988.

[8] R. King-Smith and D. Vanderbilt, "Theory of polarization of crystalline solids," *Physical Review B*, vol. 47, no. 3, p. 1651, 1993.

[9] R. Resta, "Macroscopic polarization in crystalline dielectrics: the geometric phase approach," *Reviews of modern physics*, vol. 66, no. 3, p. 899, 1994.

[10] R. Resta and S. Sorella, "Electron localization in the insulating state," *Physical Review Letters*, vol. 82, no. 2, p. 370, 1999.

[11] D. J. Thouless, M. Kohmoto, M. P. Nightingale, and M. den Nijs, "Quantized hall conductance in a two-dimensional periodic potential," *Physical review letters*, vol. 49, no. 6, p. 405, 1982.

[12] M. Kohmoto, "Topological invariant and the quantization of the hall conductance," *Annals of Physics*, vol. 160, no. 2, pp. 343–354, 1985.

[13] B. A. Bernevig, T. L. Hughes, and S.-C. Zhang, "Quantum spin hall effect and topological phase transition in hgte quantum wells," *science*, vol. 314, no. 5806, pp. 1757–1761, 2006.

[14] T. Thonhauser and D. Vanderbilt, "Insulator/chern-insulator transition in the haldane model," *Physical Review B*, vol. 74, no. 23, p. 235111, 2006.

[15] S. Patankar, L. Wu, B. Lu, M. Rai, J. D. Tran, T. Morimoto, D. E. Parker, A. G. Grushin, N. Nair, J. Analytis, *et al.*, "Resonance-enhanced optical nonlinearity in the weyl semimetal taas," *Physical Review B*, vol. 98, no. 16, p. 165113, 2018.

[16] N. Marzari and D. Vanderbilt, "Maximally localized generalized wannier functions for composite energy bands," *Physical review B*, vol. 56, no. 20, p. 12847, 1997.

[17] N. Marzari, A. A. Mostofi, J. R. Yates, I. Souza, and D. Vanderbilt, "Maximally localized wannier functions: Theory and applications," *Reviews of Modern Physics*, vol. 84, no. 4, p. 1419, 2012.

[18] I. Souza, T. Wilkens, and R. M. Martin, "Polarization and localization in insulators: Generating function approach," *Physical Review B*, vol. 62, no. 3, p. 1666, 2000.

[19] K. Binder, "Theory of first-order phase transitions," *Reports on progress in physics*, vol. 50, no. 7, p. 783, 1987.

[20] K. Binder, "Critical properties from monte carlo coarse graining and renormalization," *Physical Review Letters*, vol. 47, no. 9, p. 693, 1981.

[21] M. E. Fisher and M. N. Barber, "Scaling theory for finite-size effects in the critical region," *Physical Review Letters*, vol. 28, no. 23, p. 1516, 1972.

[22] W. Selke, "Critical binder cumulant of two-dimensional ising models," *The European Physical Journal B-Condensed Matter and Complex Systems*, vol. 51, no. 2, pp. 223–228, 2006.

[23] B. Hetényi, M. H. Müser, and B. Berne, "Second-order reentrant phase transition in the quantum anisotropic planar rotor model," *Physical review letters*, vol. 83, no. 22, p. 4606, 1999.

[24] R. Resta, "Quantum-mechanical position operator in extended systems," *Physical Review Letters*, vol. 80, no. 9, p. 1800, 1998.

[25] M. Gell-Mann and F. E. Low, "Quantum electrodynamics at small distances," *Physical Review*, vol. 95, no. 5, p. 1300, 1954.

[26] C. G. Callan Jr, "Broken scale invariance in scalar field theory," *Physical Review D*, vol. 2, no. 8, p. 1541, 1970.

[27] B. Hetényi, S. Parlak, and M. Yahyavi, "Scaling and renormalization in the modern theory of polarization: Application to disordered systems," *Physical Review B*, vol. 104, no. 21, p. 214207, 2021.

[28] W. Su, J. Schrieffer, and A. J. Heeger, "Solitons in polyacetylene," *Physical review letters*, vol. 42, no. 25, p. 1698, 1979.

[29] J. W. Demmel, *Applied numerical linear algebra*. SIAM, 1997.

[30] L. P. Kadanoff, "Scaling laws for ising models near t c," *Physics Physique Fizika*, vol. 2, no. 6, p. 263, 1966.

Appendix A

Taylor expansion of characteristic function is,

$$\ln Z_1 = \sum_{n=1}^{\infty} \left(\frac{2\pi i}{L}\right)^n \frac{C_n}{n!} \tag{A.1}$$

Expansion of second cumulant definition given by Resta-Sorella follows,

$$\begin{aligned}\left(\frac{L}{2\pi i}\right)^2 2\,\mathrm{Re}\ln Z_1 &= \left(\frac{L}{2\pi i}\right)^2 2\,\mathrm{Re}\left(\sum_{n=1}^{\infty}\left(\frac{2\pi i}{L}\right)^n \frac{C_n}{n!}\right) \\ &= \left(\frac{L}{2\pi i}\right)^2 2 \sum_{n=2,4,6,\ldots}^{\infty}\left(\frac{2\pi i}{L}\right)^n \frac{C_n}{n!} \\ &= C_2 + \left(\frac{2\pi i}{L}\right)^2 \frac{C_4}{12} + \mathcal{O}(L^{-4})\end{aligned} \tag{A.2}$$

When second cumulant proposed with alternative way to express is expanded, it yields,

$$\left(\frac{L}{2\pi i}\right)^2 2(\tilde{Z}_1 - 1) = \left(\frac{L}{2\pi i}\right)^2 2(Z_1 e^{-i\,\mathrm{Im}\ln Z_1} - 1) \tag{A.3}$$

$$\begin{aligned}
&= \left(\frac{L}{2\pi i}\right)^2 2\left(\exp\left(\sum_{m=1}^{\infty}\left(\frac{2\pi i}{L}\right)^m \frac{C_m}{m!}\right)\exp\left(-iIm\sum_{n=1}^{\infty}\left(\frac{2\pi i}{L}\right)^n \frac{C_n}{n!}\right) - 1\right) \\
&= \left(\frac{L}{2\pi i}\right)^2 2\left(\exp\left(\sum_{m=1}^{\infty}\left(\frac{2\pi i}{L}\right)^m \frac{C_m}{m!}\right)\exp\left(-\sum_{n=1,3,5,\ldots}^{\infty}\left(\frac{2\pi i}{L}\right)^n \frac{C_n}{n!}\right) - 1\right) \\
&= \left(\frac{L}{2\pi i}\right)^2 2\left(\exp\left(\sum_{m=1}^{\infty}\left(\frac{2\pi i}{L}\right)^{2m} \frac{C_{2m}}{(2m)!}\right) - 1\right) \\
&= \left(\frac{L}{2\pi i}\right)^2 2\left(\sum_{t=0}^{\infty}\left(\sum_{m=1}^{\infty}\left(\frac{2\pi i}{L}\right)^{2m} \frac{C_{2m}}{(2m)!}\right)^t \frac{1}{t!} - 1\right) \\
&= C_2 + \left(\frac{2\pi i}{L}\right)^2 \frac{C_4}{12} + \left(\frac{2\pi i}{L}\right)^2 \frac{C_2^2}{4} + \mathcal{O}(L^{-4})
\end{aligned}$$